AGU PUBLICATIONS

JGR

Journal of Geophysical Research: Oceans

RESEARCH ARTICLE
10.1002/2015JC011560

Special Section:
Physical Processes Responsible for Material Transport in the Gulf of Mexico for Oil Spill Applications

Asymmetric oceanic response to a hurricane: Deep water observations during Hurricane Isaac

Laura J. Spencer[1], Steven F. DiMarco[1,2], Zhankun Wang[3,4], Joseph J. Kuehl[5], and David A. Brooks[1]

[1]Department of Oceanography, Texas A&M University, College Station, Texas, USA, [2]Geochemical and Environmental Research Group, Texas A&M University, College Station, Texas, USA, [3]National Centers for Environmental Information, NOAA, Silver Spring, Maryland, USA, [4]Earth System Science Interdisciplinary Center, University of Maryland, College Park, Maryland, USA, [5]School of Engineering and Computer Science, Baylor University, Waco, Texas, USA

Key Points:
- The oceanic response to hurricane forcing is asymmetric with respect to the storm's trajectory
- Oceanic response was limited to about 15 inertial periods

Correspondence to:
S. F. DiMarco,
sdimarco@tamu.edu

Citation:
Spencer, L. J., S. F. DiMarco, Z. Wang, J. J. Kuehl, and D. A. Brooks (2016), Asymmetric oceanic response to a hurricane: Deep water observations during Hurricane Isaac, *J. Geophys. Res. Oceans*, *121*, 7619–7649, doi:10.1002/2015JC011560.

Received 14 DEC 2015
Accepted 14 JUL 2016
Accepted article online 18 JUL 2016
Published online 19 OCT 2016

Abstract The eye of Hurricane Isaac passed through the center of an array of six deep water water-column current meter moorings deployed in the northern Gulf of Mexico. The trajectory of the hurricane provided for a unique opportunity to quantify differences in the full water-column oceanic response to a hurricane to the left and right of the hurricane trajectory. Prior to the storm passage, relative vorticity on the right side of the hurricane was strongly negative, while on the left, relative vorticity was positive. This resulted in an asymmetry in the near-inertial frequencies oceanic response at depth and horizontally. A shift in the response to a slightly larger inertial frequencies $\sim 1.11f$ was observed and verified by theory. Additionally, the storm passage coincided with an asymmetric change in relative vorticity in the upper 1000 m, which persisted for ~15 inertial periods. Vertical propagation of inertial energy was estimated at 29 m/d, while horizontal propagation at this frequency was approximately 5.7 km/d. Wavelet analysis showed two distinct subinertial responses, one with a period of 2–5 days and another with a period of 5–12 days. Analysis of the subinertial bands reveals that the spatial and temporal scales are shorter and less persistent than the near-inertial variance. As the array is geographically located near the site of the Deep Water Horizon oil spill, the spatial and temporal scales of response have significant implications for the fate, transport, and distribution of hydrocarbons following a deep water spill event.

1. Introduction

Tropical storm Isaac entered the Gulf of Mexico on 27 August 2012 and strengthened to become a Category 1 hurricane on 28 August [*Jaimes and Shay*, 2015]. Hurricane Isaac passed directly over a deep water current-meter mooring array deployed along the continental slope in the Mississippi Fan region of the northern Gulf of Mexico hours before making landfall in southern Louisiana on 29 August 2012 (Figure 1). Acoustic Doppler Current Profilers and current meters deployed in the mooring array measured the oceanic response to the passage of this hurricane with two of the six moorings covering the full water column. The bathymetry of the northern Gulf of Mexico and vertical positions of mooring instrumentation are shown in Figure 2.

Moored currents and wave measurements taken directly under hurricanes during their passage are difficult to obtain due to the unpredictability of the locations that hurricanes will appear and the paths they will follow [*Shay et al.*, 1989]. Most moored measurements of hurricanes have been chance encounters by instruments deployed for other scientific purposes [e.g., *Brooks*, 1983; *Teague et al.*, 2007; *Wang et al.*, 2012], as was the case in this study. The relatively tight grid pattern, 30 km spacing, of the mooring array and the full water-column measurements make this study ideal for investigating the oceanic response to a hurricane. The processes observed in the current velocity data collected during the hurricane include deterministic background tidal variability, background eddy fields circulation patterns associated with the Loop Current and eddies at the time of the storm, and near-inertial and subinertial variability that is initiated as a response to the storm. Many studies have investigated the oceanic response to hurricanes captured by moored arrays in the Gulf of Mexico [*Brooks*, 1983; *Shay et al.*, 1989; *Teague et al.*, 2007; *Zheng et al.*, 2006; *Hamilton*, 1990; *Oey et al.*, 2008]. The uniqueness of the data set presented here is that the eye of this hurricane passed through the center of the array with three moorings to the right and three to the left of the

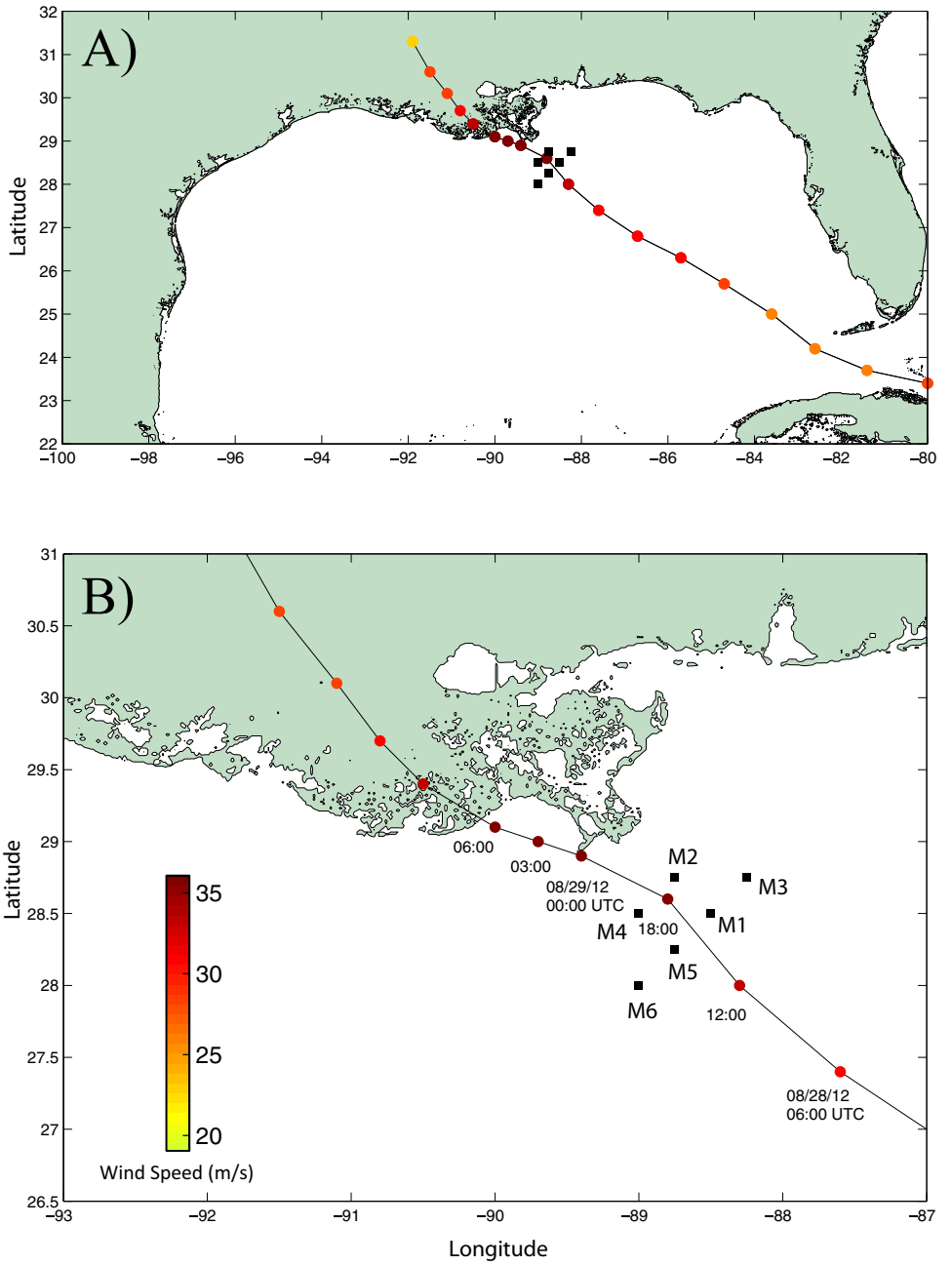

Figure 1. Hurricane Isaac Track. (A) Track of Hurricane Isaac in the Gulf of Mexico. (B) Track of Hurricane Isaac over the GISR mooring array (black squares). Hurricane track points are colored according to reported wind speed in m/s.

hurricane track, which is similar to the study of 2004 hurricane Ivan by *Teague et al*. [2007], but over the continental slope.

The density structure of the water column combined with the circulation patterns can affect how energy can propagate through the water column after an extreme event such as a hurricane. The relative vorticity of the region can also affect the frequency of the inertial response to either above (in cyclonic background flow) or below (in anticyclonic flow) the local inertial frequency [*Mooers*, 1975; *Kunze*, 1985]. Asymmetrical sea surface cooling has been observed following the passage of hurricanes, where the right side of the hurricane track experiences a greater amount of heat loss compared to the left side of the hurricane track. This asymmetrical sea surface cooling implies a typical pronounced rightward bias in the current response [*Church et al*., 1989; *Sanford et al*., 1987; *Shay et al*., 1992, 1998]. Numerical ocean models have been used to

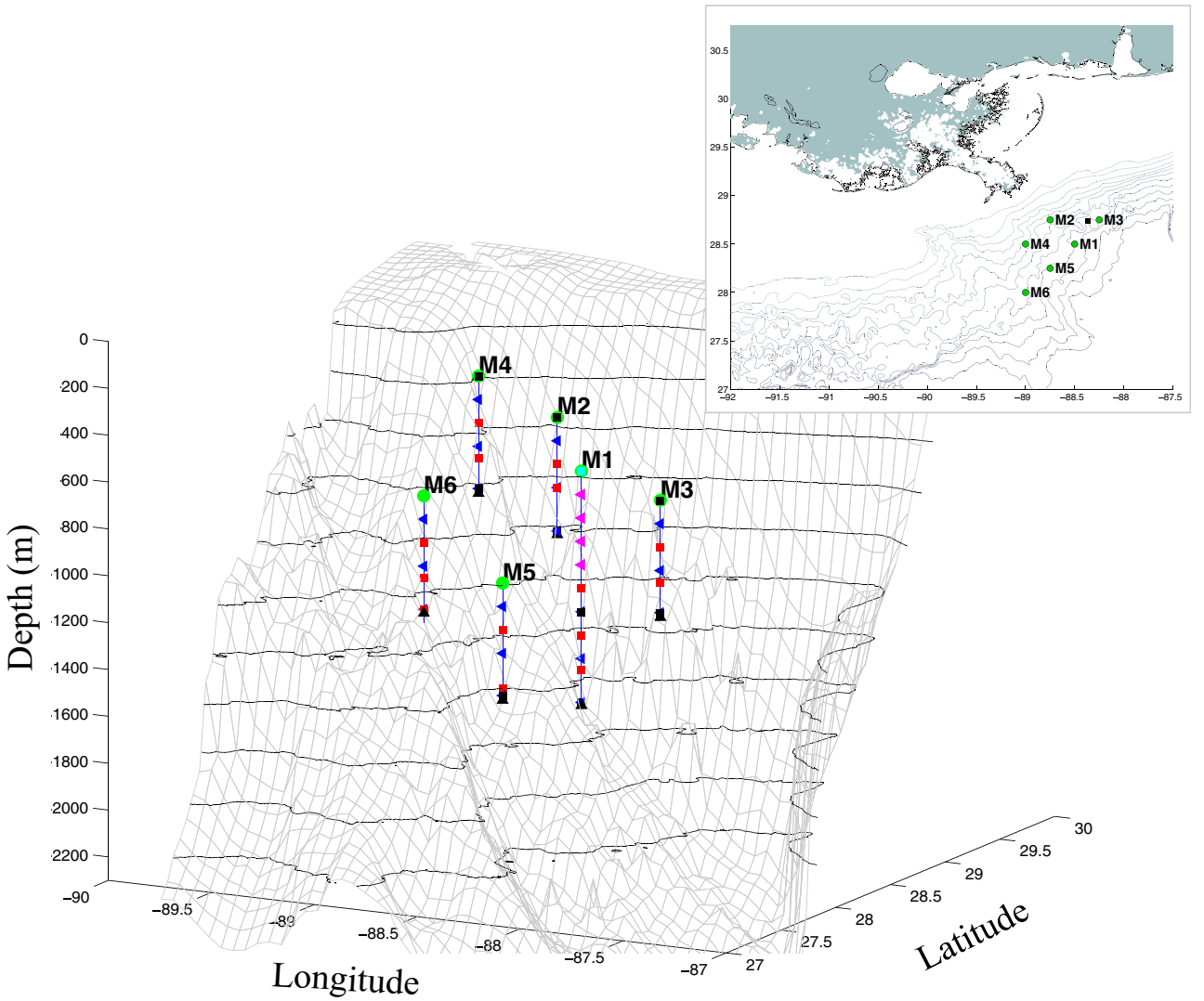

Figure 2. 3-D basemap of mooring array. M1 (28.5′N, 88.5′W), M2 (28.75′N, 88.75′W), M3 (28.75′N, 88.25′W), M4 (28.5′N, 89′W), M5 (28.25′N, 88.75′W), M6 (28′N, 89′W). Green circles: upward looking 75 kHz ADCPs; purple triangles: InterOcean S4A; red squares: RCM 11 or RCM 8; blue triangle: SBE-37 Microcat or SBE16 CTD; black squares: StarMon themistors; and black triangles: Benthos 685A. The depths of instruments are listed in Table 1. The inset basemap shows the location of the mooring array relative to the coastline. Bathymetry lines are shown every 200 m beginning at 200 m and ending at 2200 m for both the 3-D and inset basemaps.

explain that the directions of the wind stress vectors are responsible for the pronounced rightward bias in the observed SST response to a hurricane [*Bender et al*., 1993; *Price*, 1983]. Note that the patchy structure of the eddy field during the hurricane passage might also have contributions to the asymmetrical sea surface cooling due to the presence of cyclonic and anticyclonic background circulations [e.g., *Jaimes and Shay*, 2009, 2010; *Jaimes et al*., 2011; *Walker et al*., 2005]. *Huong and Oey* [2015] report a spatially asymmetric biological response to the passage of a tropical cyclone in the western Pacific.

Strong near-inertial oscillations generated by storms have been observed in current meter data in the Gulf of Mexico, Atlantic, Pacific, and Indian Ocean [*Brooks*, 1983; *Qi et al*., 1995; *Shay and Elsberry*, 1987; *Shay and Chang*, 1997; *Shay et al*., 1998; *Wang et al*., 2012]. Subinertial oscillations (2–10 days periods) have been observed in moored current meter data in response to Tropical Cyclone Gonu in the Northern Arabian Sea [*Wang et al*., 2012] and subinertial oscillations with 2–5 day periods were observed in moored current meter data in response to Hurricane Ivan in the northeastern Gulf of Mexico [*Teague et al*., 2007].

Using airborne ocean profilers data collected during the intensification of Isaac from tropical storm to a Category 1 hurricane, *Jaimes and Shay* [2015] investigated the upwelling, downwelling, and warming responses

Table 1. Mooring Instrumentation and Vertical Placement

Mooring	Latitude	Longitude	Total Water Depth	75 kHz ADCP Depth	SBE-16 CTD Depth	InterOcean S4A Depth	StarMon Temp Depth	RCM-8 Depth	RCM-11 Depth	SBE-37 Microcat Depth	Benthos 685A Depth
1	28.50N	88.50W	1690m	690m	692m	790m	1190m		1290m	1292m	1690m
						890m	1390m		1490m	1679m	1690m
						990m	1540m		1677m		
						1090m					
2	28.75 N	88.75 W	1035m	535m			*735m*		*635m*	*537m*	1035m
							837m		*835m*	1022m	1035m
									1020m		
3	28.75 N	88.25 W	1337m	837m			1037m		937m	839m	1337m
							1187m		1137m	1319m	1337m
									1317m		
4	28.50 N	89.00 W	836m	336m			536m		436m	338m	836m
							686m		636m	818m	836m
									816m		
5	28.25 N	88.75 W	1650m	1150m			1350m	1450m	1250m	1632m	1650m
							1500m		1630m		1650m
6	28.00 N	89.00 W	1312m	812m			1012m	1112m	912m		1312m
							1162m		1297m		1312m
							1299m				

to Hurricane Isaac. The predominantly downwelling responses over warm, anticyclonic mesoscale oceanic features interact with the storm during the intensification of Isaac and prevent significant cooling of the sea surface, and Isaac rapidly attains and maintains hurricane status. They conclude that elucidating downwelling responses is critical to better understanding tropical storm intensification over warm mesoscale oceanic features. Unlike *Jaimes and Shay* [2015] which focuses on the intensification of tropical storm Isaac to hurricane, this paper will focus on the impact of Isaac on the physical structure of the Gulf of Mexico by determining the metrics of the storm's impact during the forced and relaxation stages and comparing these metrics to previous observations and contrasting the oceanic response to the right and to the left of the hurricane track.

The metrics of the oceanic response observed in the data will be described including the vertical and horizontal propagation speeds of the near-inertial oscillations, the phase propagation directions of the oscillations, the group velocities of these waves, the relationships between the oscillations observed at different depth levels, and the difference in these metrics relative to the position of the hurricane and its track. The relative vorticity of the region is calculated and used to evaluate the effect of vorticity on the current response to Hurricane Isaac.

This research is funded by the Gulf Integrated Spill Research Consortium as one of seven consortia funded by the Gulf of Mexico Research Initiative. A major goal of the Gulf Integrated Spill Research Project is to validate and improve oil spill transport and transformation prediction using the numerical circulation models that use data collected near the Deep Water Horizon oil spill site. The description of the oceanic response to a hurricane event will help to improve the model's capability to capture the near-inertial and subinertial responses from future extreme events in the Gulf of Mexico by utilizing the metrics determined from Hurricane Isaac.

2. Materials and Methods

2.1. Data

The data used in this analysis were obtained from instrumentation deployed on six deep water moorings deployed in the Gulf of Mexico. Each mooring featured an upward looking RDI 75 kHz Long Ranger acoustic current Doppler profiler (ADCP) at the top of the mooring. Addition instrumentation included InterOcean S4A single point current meters, Aanderaa record current meters, SeaBird SBE-37 Microcat CTDs, and StarMon temperature sensors. Table 1 summarizes the mooring array instrumentation and placement. Hydrographic data for the mooring region were collected on the G01 mooring deployment cruise in July 2012. Temperature, conductivity, and pressure profiles from deployments of a SeaBird 911*plus* were collected in a grid pattern around the mooring deployment site during the deployment (G01), servicing (G04), and

recovery cruises (G06). The data from the CTD casts were used to determine the hydrographic conditions for the region before the storm including the stratification of the water column.

Hurricane wind and track positional data were obtained from NOAA's National Hurricane Center (NHC) archives for Hurricane Isaac found at ftp://ftp.nhc.noaa.gov/atcf/archive/2012. NHC has conducted comprehensive analyses with the goal to provide the best storm track data. The wind speed and surface pressure data are a best fit calculated from observations of the hurricane from satellites, aircraft, and radar, ships, land stations, and buoys. Doppler radar data from the National Weather Service, Météo-France, and the Institute of Meteorology of Cuba were also used to make center fixes and help track the center of Isaac through the Gulf of Mexico.

2.1.1. Quality Control

The current meter was quality-controlled in accordance with the procedures outlined in the MMS Quality Control Analysis report for ADCP data [*Bender and DiMarco*, 2009]. The quality-controlled data were originally recorded at 30 min intervals from the ADCPs and at hourly intervals from the other current meters. After quality control procedures including the removal of flagged data, the removal of extreme outlier, and gap filling were applied to each data set, all records were subsampled using linear interpolation to a consistent hourly grid to allow for comparison between records. A cosine-Lanczos filter was used to obtain band passed records of the data [*Emery and Thomson*, 2001]. A 40 h low-pass (LP) filter was applied to each of the velocity data records to remove tidal and inertial variability. The 40 h LP filtered data were used to identify and quantify the subinertial oscillations present in each record using wavelet analysis. All data records were band-pass filtered between 0.8*f* to 1.2*f*, with *f* being the local Coriolis parameter, to isolate the near-inertial energy band. A 2–5 days period band and a 5–12 days period band were partitioned from each time series to isolate the corresponding subinertial waves that are identified from the time series wavelet analysis.

The moorings were deployed near a critical latitude, defined as 30°N or 30°S, meaning that local inertial period, approximately 24 h, is very near the local diurnal tidal period [*DiMarco et al.*, 2000; *Zhang et al.*, 2008]. Harmonic analysis is used to remove the tidal frequencies as described in *DiMarco and Reid* [1998]. The quality-controlled data were detided to remove the eight principal tidal constituents using the iterated least squares method of cyclic descent [*Bloomfield*, 1976; *DiMarco and Reid*, 1998]. Due to the extreme hurricane event in this relatively short time series, the currents recorded during the storm event were identified and removed before fitting the tidal oscillations to the time series.

2.2. Methods

2.2.1. Wind Stress

Output from the NOAA gridded atmospheric observations were used to calculate wind stress and wind stress curl for the hurricane track (near Mooring 1) and on each side of the hurricane track. First, wind speed was calculated from the velocity components, and the wind drag coefficient C_D was estimated based on recent results from field experiments in hurricanes [*Powell et al.*, 2003; *Black et al.*, 2007], where C_D is given by the same formula used in *Jaimes and Shay* [2015]:

$$C_D = \begin{cases} (4-0.6W_{10})\times 10^{-3} & \text{for } W_{10} < 5ms^{-1} \\ (0.7375+0.0525W_{10})\times 10^{-3} & \text{for } 5ms^{-1} \le W_{10} < 25ms^{-1} \\ 2.05\times 10^{-3} & \text{for } W_{10} \ge 25ms^{-1} \end{cases}$$

W_{10} is the wind speed magnitude at a height of 10 m in m/s. The zonal and meridional wind stress components were calculated according to the equation presented by *Nelson and United States National Marine Fisheries Service* [1977]

$$(\tau_x,\ \tau_y) = \rho_a C_D(|W_{10}|U_{10}, |W_{10}|V_{10}),$$

where ρ_a is the density of air (1.22 kg/m^3) and U_{10} and V_{10} are the eastward and northward components of the wind velocity measured at a height of 10 m obtained from the gridded observations. The resulting wind stress components were used to compute the curl of the wind stress at the mooring site and on each side of the hurricane track. The wind stress and wind stress curl time series were calculated for the mooring area at the location of Mooring 1 (28.5′N, 88.5′W), for the right side of the storm 102 km northeast of Mooring 1 at (27.75′N, 89.25′W), and for the left side of the storm 102 km southwest of Mooring 1 at (29.25′N, 87.75′W).

2.2.2. Wavelets

Wavelet analysis is used to obtain time histories of amplitudes of specific frequency bands within a time series record. The wavelet analysis software package developed by *Torrence and Compo* [1998] is used on current velocity records, http://paos.colorado.edu/research/wavelets. A Morlet basis function was used to generate wavelet power spectra for each ADCP and current meter record. Scale-averaged wavelet power in the inertial band (0.8*f* to 1.2*f*) and the subinertial bands (2–5 and 5–12 days) were generated to provide time series of amplitude and phase of the spectral bands. Additionally, a correction to the original software package is applied as suggested in *Liu et al*. [2007].

Coherence analysis was performed on selected current velocity pairs to estimate spectral coherence and relative phase by frequency [*Emery and Thomson*, 2001]. Wavelet coherence analysis utilizes a cross wavelet transform and wavelet coherence to examine relationships in time frequency space between two time series. The cross wavelet transform exposes regions with high common power and further reveals information about the phase relationship between two signals. If two signals share a large common power and have a consistent phase relationship then a possible causality between the time series is suggested [*Grinsted et al*., 2004]. In this study, wavelet coherence analysis was used to compare two velocity time series records at a specific location or a similar depth level in order to determine periods of strong coherency and phase differences between the two records.

2.2.3. Vertical Relative Vorticity

Relative vorticity is the measure of the rotation of the ocean relative to the background vorticity due to the rotation of the Earth, or planetary vorticity. The definition of vertical relative vorticity is $\zeta_z = \delta v/\delta x - \delta u/dy$, where u and v are the horizontal velocity components in the x and y directions, respectively [*Emery and Thomson*, 2001] and z indicates that this is the vertical component of the three-dimensional vorticity. We have assumed that the flow is mainly two-dimensional since this is a relatively large-scale analysis. Regions of positive relative vorticity in the ocean correspond to cyclonic circulation in the Northern Hemisphere, and regions of negative relative vorticity correspond to anticyclonic circulation. Relative vorticity for the right side of the hurricane track was calculated from current meter data at Moorings 1–3 at all available depths between 245 and 452 m. Due to the deep deployment of Mooring 5 in contrast to Moorings 4 and 6, the current meter records from Moorings 4 and 6 are used with Mooring 1 to estimate the relative vorticity on the left side of the hurricane track at all available depths between 187 and 291 m as well as 436 and 636 m. The relative vorticity was calculated hourly for a triangular array by approximating the circle integration by a discrete sum of the radial and normal velocity components along the circle connecting the three moorings according to the methods described in *Müller et al*. [1988]. The relative vorticity estimates for each side of the hurricane was compared with altimetry records and current meter records to determine how relative vorticity relates to oceanic response to Hurricane Isaac.

2.2.4. Hurricane Parameters

Air-sea interaction in hurricanes can be compactly described by a few fundamental variables such as the average translation speed of the storm U_h, the radius of maximum wind speed R_{max}, the maximum wind stress τ_{max}, the inertial frequency of the region *f*, and the reduced gravitational acceleration g' [*Price et al*., 1994]. Several nondimensional parameters can also be derived from these fundamental variables in order to describe the oceanic response to the storm. These parameters include the nondimensional storm speed S, the thermocline Burger number B, and the Rossby number for the mixed layer current Q.

$$S = \pi U_h/4fR_{max}, \tag{1}$$

$$B = g'h_1/4f^2R^2_{max}, \tag{2}$$

$$Q = \tau_{max}/\rho_o h_1 U_h f, \tag{3}$$

where ρ_o is the density of seawater and h_1 is depth of mixed layer.

The nondimensional storm speed S is the ratio of the local inertial period to the hurricane residence time. The thermocline Burger number B is a direct measure of the pressure coupling between the mixed layer current and the thermocline current. The Rossby number Q is the ratio of horizontal advection of momentum to the Coriolis force. The derivations of these nondimensional parameters are described in *Price et al*. [1994].

2.2.5. Water Column Response

The measure of stratification or stability in the water column is important to determine the group velocities of the inertial response to Hurricane Isaac. The Brunt-Väisälä frequency (N), or buoyancy frequency, is the natural frequency of oscillation of a parcel of water displaced vertically from its level of equilibrium. In the ocean, larger values of N correspond to a more stable water column. The Brunt-Väisälä frequency is defined as:

$$N = [-(g/\rho)(\delta\rho/\delta z)]^{1/2}, \tag{4}$$

where g is gravitational acceleration, z is depth, and ρ is the potential density calculated using the potential temperature, salinity, and pressure profiles.

A total of 36 CTD casts were taken on the G01 cruise. Of these, 18 casts were taken within 25 km of any mooring deployment site. These 18 casts are used to estimate the stratification of the water column before the passage of the hurricane. Note that the G01 mooring deployment cruise was in early July 2012 approximately 2 months before the storm. The G01 data may not be the best estimate of the pre-storm stratification condition in the study region in summer 2012, but this is the closest data set we can find. Those moorings only measured water density in the lower water column at several fixed depths, which is insufficient to characterize the stratification during the Isaac. The Brunt-Väisälä frequency estimated from G01 data will be used with estimations of vertical and horizontal scales to calculate group velocities of near-inertial oscillations observed in the wake of Hurricane Isaac (Category 1 in the Saffir-Simpson scale).

Estimations of the vertical and horizontal scales of the near-inertial oscillations are determined by observing the phase shift of current meter amplitudes between different depth levels at a single mooring and between similar depth levels from two separate moorings, respectively. The speed of the energy propagation is determined by dividing the phase shift measured in time units by the known distance between the observations. When the frequency of the energy f_{eff} is known (i.e., the effective frequency) and the speed of the energy C is calculated from the known distance traveled over time, the scale (or wavelength L) is determined from $\mathrm{L} = \mathrm{C} \times f_{eff}^{-1}$.

Using the vertical and horizontal scale estimates, the horizontal and vertical group speeds for the near-inertial response are calculated using equations (5a) and (5b) from *Brooks* [1983]. For N^2 constant, we can determine the group speeds, or energy transport velocity vectors:

$$\mathrm{C_{gy}} = \omega l^{-1}(N\omega^{-1}\tan\theta)^2, \tag{5a}$$

$$\mathrm{C_{gz}} = -\omega m^{-1}(N\omega^{-1}\tan\theta)^2, \tag{5b}$$

in terms of the phase velocity vector,

$$\mathrm{C_p} = (\omega l^{-1}, \ \omega m^{-1}), \tag{6}$$

where ω is the effective Coriolis frequency and l and m are the horizontal and vertical wavenumbers calculated from the length scales as

$$(l, m) = 2\pi(\mathrm{L_y}^{-1}, \mathrm{L_z}^{-1}). \tag{7}$$

N is the estimated Brunt-Väisälä frequency calculated from the CTD profiles taken during the mooring deployment cruise. The tilt of the phase distribution with depth, or the angle between the phase vectors and the vertical θ can be determined directly from the length scales as

$$\tan\theta = lm^{-1}, \tag{8}$$

and estimated from the dispersion relation as

$$\tan\theta = N^{-1}(\omega^2 - f^2)^{1/2}, \tag{9}$$

where ω is the observed frequency of the near-inertial response and f is the Coriolis parameter. As explained in *Brooks* [1983], depth-leading phases are indicative of downward propagation of energy into the thermocline. From (5b), the kinetic energy propagates vertically with the opposite sense of the phase propagation.

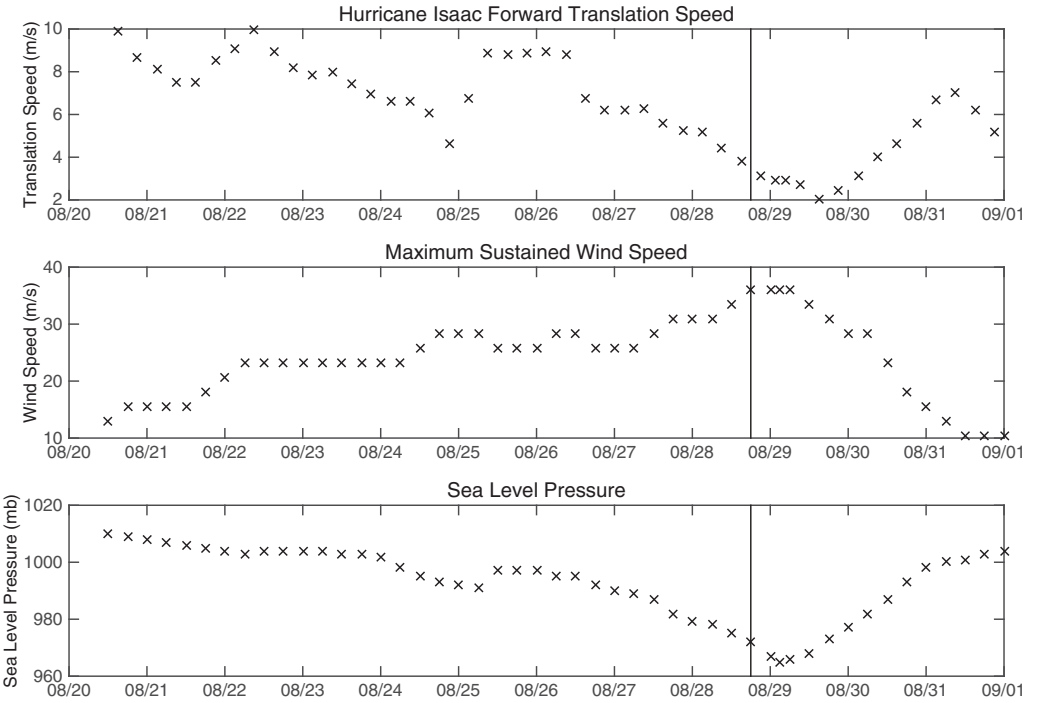

Figure 3. Hurricane Isaac translation speed, wind speed, and sea level pressure. (A) Hurricane Isaac forward translation speed in m/s calculated from reported storm track positions; (B) maximum sustained wind speed for Hurricane Isaac in m/s; (C) sea level pressure during Hurricane Isaac. Red vertical lines represent closest approach of Hurricane Isaac to GISR mooring array. All times are reported in UTC. Storm track positions, wind speed, and sea level pressure values were reported by Nation Hurricane Center and downloaded from ftp://ftp.nhc.noaa.gov/atcf/archive/2012/.

In order for energy to propagate downward into the thermocline, the phase vector must be tipped slightly out of the vertical.

3. Results

Hurricane Isaac passed directly over the center of the mooring array before making its first of two landfalls along the coast of Louisiana, the first at Southwest Pass at around 0000 UTC on 29 August, then again just west of Port Fourchon, Louisiana approximately 8 h later. Maximum sustained wind speeds of 36.01 m/s were recorded with Hurricane Isaac's first landfall at Southwest Pass [*Berg*, 2013]. The translation speed of Hurricane Isaac as it passed over the mooring array was approximately 3.5 m/s based on reported times and locations of the center of the storm. Figure 1a shows the hurricane track in the Gulf of Mexico, and Figure 1b shows the path of Hurricane Isaac as it passed over the GISR mooring array before and after making landfall. Figure 3 presents a time series of the reported storm wind speeds and sea level pressure and the calculated translation speeds during the storm's passage over the mooring array. As the storm passed the array, the sea level pressure at the storm's center was decreasing and was below 980 mb.

3.1. Scales and Parameters

The fundamental variables and the derived nondimensional parameters as described in section 2.2.4 for Hurricane Isaac are presented in Table 2. We have included the same previously published variables for Hurricanes Ivan, Norbert, Frederic, and Gilbert in Table 2. Hurricane Ivan struck the Gulf of Mexico in September 2004 as a Category 4 hurricane before making landfall near Gulf Shores, Alabama. Hurricane Ivan passed directly over a mooring array of 14 ADCPs deployed in the DeSoto Slope as part of the Slope to Shelf Energetics and Exchange Dynamics (SEED) project conducted by the Naval Research Laboratory [*Teague et al.*, 2007]. Hurricane Norbert originated in the Pacific Ocean west of the Mexican coast and peaked in strength as a Category 4 hurricane before weakening back into a tropical storm and striking the Baja California Peninsula in September 1984. Aircraft deployed AXCPs captured currents near the storm's center providing a quasi-synoptic view of the response to Hurricane Norbert [*Price et al.*, 1994]. Hurricane Frederic struck the

Table 2. Hurricane Parameters[a]

Parameter	Isaac (2012)	Ivan (2004)	Norbert (1984)	Frederic (1979)	Gilbert (1988)
U_h (Translation Speed)	3.83 m/s	5.8 m/s	3.0 m/s	6-7 m/s	5.6 m/s
R_{max} (Cross Track Scale)	92.6 km	40 km	20 km	27-33 km	60 km
L_i (Along Track Scale)	55.03 km	81 km	62.5 km	–	–
τ_{max} (Wind Stress)	1.35 N/m^2	6.7 N/m^2	4.0 N/m^2	–	4.2 N/m^2
f (Coriolis Parameter)	6.9 x10^{-5} rad/s	7.2 x10^{-5} rad/s	4.8 x10^{-5} rad/s	7.2 x10^{-5} rad/s	5.8 x10^{-5} rad/s
g′ (Reduced Gravity)	.04 m/s^2	.04 m/s^2	.04 m/s^2	.022 m/s^2	.0286 m/s^2
h_1 (Mixed Layer Depth)	40-50 m	50 m	40 m	40-50 m	35 m
S (Non-dimensional Storm Speed)	0.47	1.6	2.4	1.4	1.04
B (Burger Number)	0.009	0.06	0.37	0.08	0.08
Q (Rossby Number)	0.13	0.55	0.7	–	–

[a]Hurricane parameters for Isaac in 2012 calculated in the study, Ivan in 2004 [*Teague et al*., 2007], Norbert in 1984 [*Price et al*., 1994], Frederic in 1979 [*Shay and Elsberry*, 1987], and Gilbert in 1988 [*Shay et al*., 1998] are presented. The mixed layer thickness used for Isaac parameter estimation is based on the density and temperature profiles of each cast from G01.

Gulf of Mexico as a Category 4 hurricane before making landfall near Dauphine Island, Alabama in September 1979. Hurricane Frederic passed within 80 km of an array of current meters in the DeSoto Canyon Region deployed by the U.S. Naval Oceanographic Office and within 150 km of an Ocean Thermal Energy Conversion mooring [*Shay and Elsberry*, 1987]. Hurricane Gilbert struck the western Gulf of Mexico in September 1988 and the primary data set used to study the upper ocean response to the hurricane was acquired during five flights in which a number of AXBTs and AXCPs were deployed [*Shay et al*., 1992]. The comparison of each of these storms to Hurricane Isaac in 2012 will be discussed later in the section 4.

3.2. Prestorm Conditions

40-HRLP velocity vector plots in Figure 4 show that in the prestorm period currents at each mooring varied in direction, with upper ocean ($z < 200$ m) currents flowing to the north and northwest at Moorings 1 and 2 and currents flowing strongly to the south at Mooring 3. Currents directions and magnitudes at Moorings 4 and 6 were variable before the storm. The current observations at all moorings are mostly consistent with the expected directions of the near-surface currents based on the available satellite altimetry for the mooring area (Figure 5). The altimetry shows a slight decrease in sea surface height that corresponds to a cyclonic feature in the area of the mooring array. This cyclonic feature is centered to the left side of the mooring array. The altimetry figures also show a slight increase in sea surface height on the right of the mooring array directly north of Mooring 3. A stronger cyclonic eddy is located to the southeast of the mooring array. The direction of flow observed at each mooring before the passage of the storm generally corresponds well with the expected flow directions based on the altimetry figures. The inconsistencies, particularly at Mooring 4, may be due to the coarseness of the spatial and temporal resolution of the altimetry figures. Each altimetry figure is a composite of 14 days of satellite data combined with an estimate of the modeled mean sea level for the Gulf of Mexico [*Leben et al*., 2002]; therefore, inaccuracies over such a small spatial scale as the moorings compared to the entire Gulf of Mexico are to be expected.

The CTD casts collected during the G01 mooring deployment cruise show the temperature and salinity relationships in the area of the moorings (Figure 6). The thermocline and mixed layer thickness is approximately 400 and 50 m, respectively, based on the density and temperature profiles of each cast (not shown). The low salinity near the surface suggests the study region can be affected by the Mississippi River plume water during summer [*Wang et al*., 2016]. Most water in the mixed layer and upper thermocline can be characterized as Gulf Common Water with salinity less than 36.4 [*Wang et al*., 2016]. However, some subtropical underwater residual might be measured during G01 cruise as salinity slightly greater than 36.5 were also measured in the upper thermocline. Brunt-Väisälä frequency profiles calculated from the CTD casts at each mooring location before deployment are shown in Figure 7. An average Brunt-Väisälä frequency profile N^2 is obtained from casts taken near the mooring locations. This average profile will be used when estimating group velocities of near-inertial internal waves observed after the hurricane. The profile indicates relatively strong stratification in the upper part of the water column above 200 m compared to the rest of the water column. Larger values of N correspond to stronger vertical density gradients in the water column.

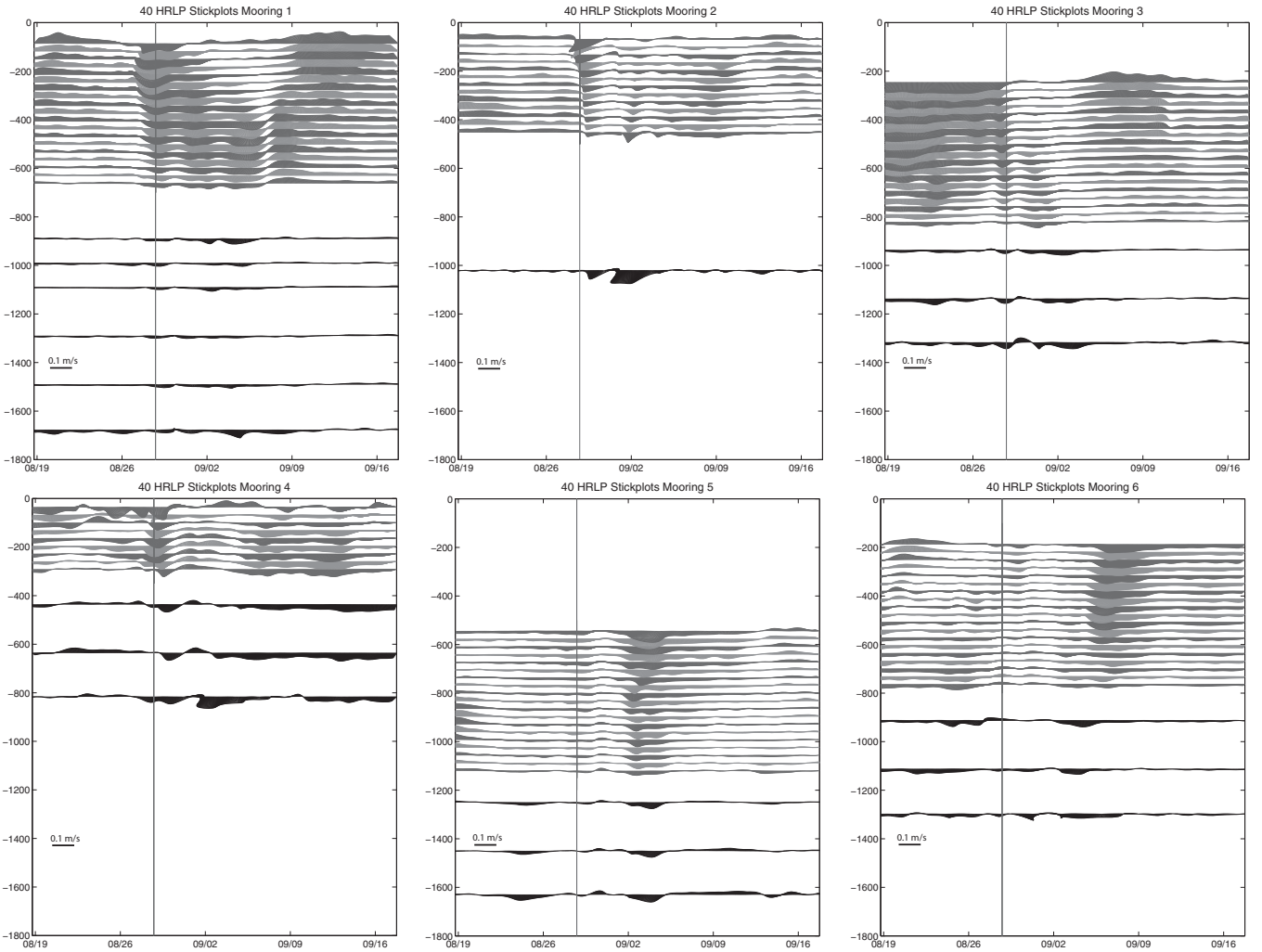

Figure 4. Velocity vector plots for 40 h low passed current meter data at each mooring 10 days before and 20 days after the passage of Hurricane Isaac are shown. The vertical red line represents the closest approach of Hurricane Isaac on 28 August 2012 at 18:00 UTC. The ADCP data are shown in alternating gray scale to provide contrast between depth layers. The black lines represent data from RCM and S4A instruments on each mooring. The direction of the vectors is oceanographic convention with currents pointing up on the page referring to currents coming from the south and flowing north. Scale on the left side of each panel indicates depth (meters) of observation for each current record.

3.3. Normalized Relative Vorticity

Vertical component of the normalized relative vorticity (hereinafter relative vorticity) time series calculated from the 40 HRLP records on each side of the hurricane track are shown in Figure 8. On the right side of the hurricane track (Moorings 1–3), the observed relative vorticity is strongly negative before the storm, which corresponds to anticyclonic circulation. On the left side of the hurricane track, the relative vorticity is positive, corresponding to cyclonic circulation, before the approach of Hurricane Isaac. On the right side of the hurricane track, the relative vorticity is negative before the storm (approximately −0.1), and then strongly increases with the passing of the cyclonic storm (from −0.15 to −0.05 within one inertial period). The relative vorticity then changes to positive approximately 5 days after the storm. The relative vorticity on the left side of the hurricane was positive (approximately 0.05) before the storm's approach. The relative vorticity remained positive for approximately 1 day after the passage of the storm before decreasing to negative relative vorticity 1 day later. The relative vorticity on the left side remained negative for about 5–7 days before returning to positive vorticity. The right side of the storm experiences the greatest change in relative vorticity as a result of Hurricane Isaac (from −0.015 to −0.05). These observed vorticity developments seem to be consistent with theoretical predictions, numerical simulations, and other observations of enhanced upwelling responses over cyclonic flow and enhanced downwelling responses over anticyclonic flow [see *Jaimes and Shay*, 2009, 2015; *Jaimes et al.*, 2011], which might provide some observational evidence to those theoretical studies.

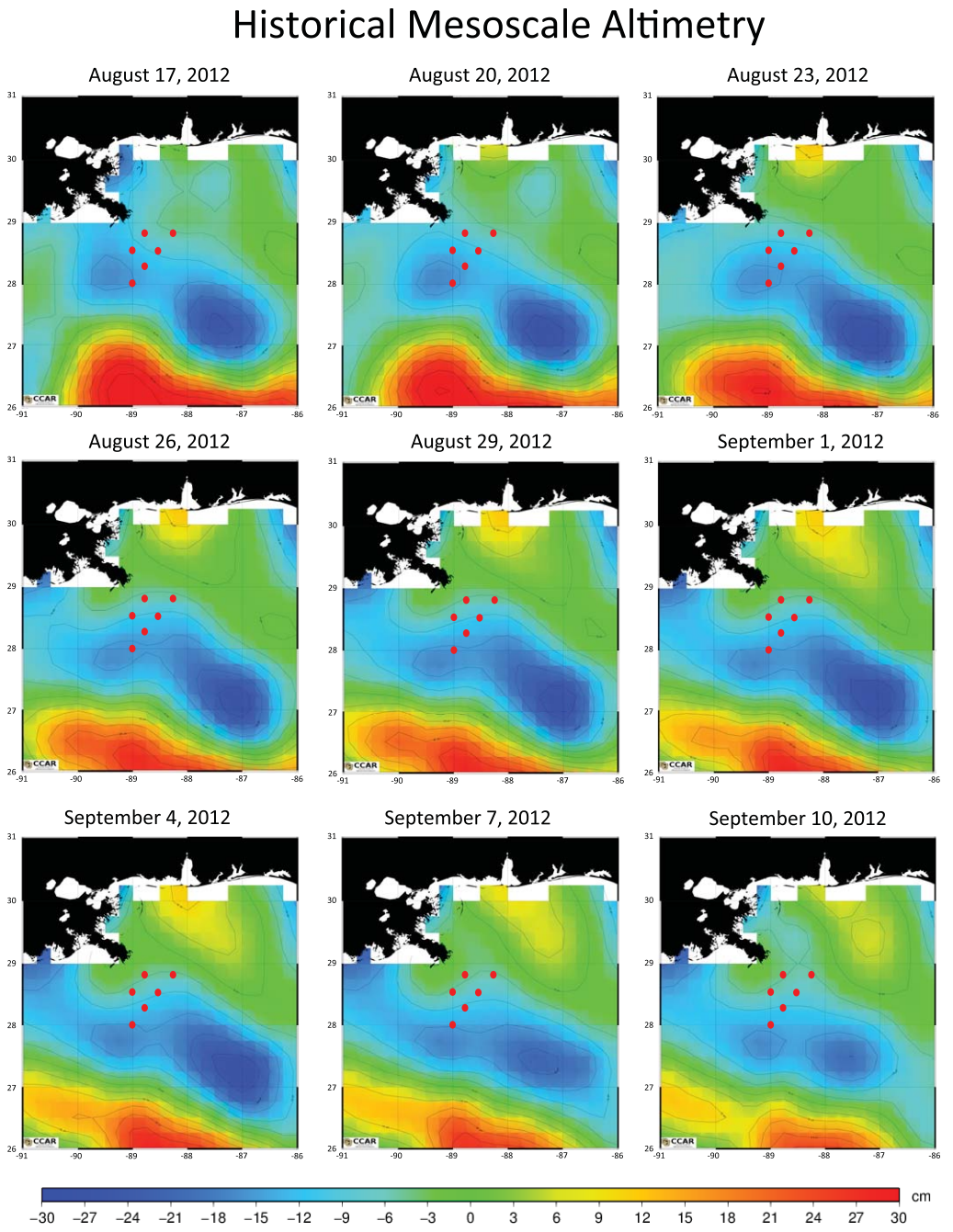

Figure 5. Historical mesoscale altimetry during Hurricane Isaac. The central panel (29 August 2012) corresponds to the closest approach of the hurricane. Altimetry figures show the estimated sea surface height in cm for the region between 26°N and 31°N and 91°W and 86°W. Red dots indicate the location of the moorings. Red (blue) colors correspond to positive (negative) sea surface heights indicating anticyclonic (cyclonic) rotation. Source: http://eddy.colorado.edu/ccar/.

The gradient of relative vorticity on the right side of the hurricane track is steeper than that on the left side as observed in Figure 9, which shows the contour plots of the relative vorticity, normalized by the local Coriolis frequency f on each side of the hurricane track.

3.4. Wind Stress/Wind Curl

The wind stress and wind stress curl for the time period near Hurricane Isaac were estimated from NOAA gridded atmospheric observations as described in section 2.2.1. The strong cyclonic signature of the hurricane is observed in the extreme wind stress vector values shown in the left column of Figure 10. The wind

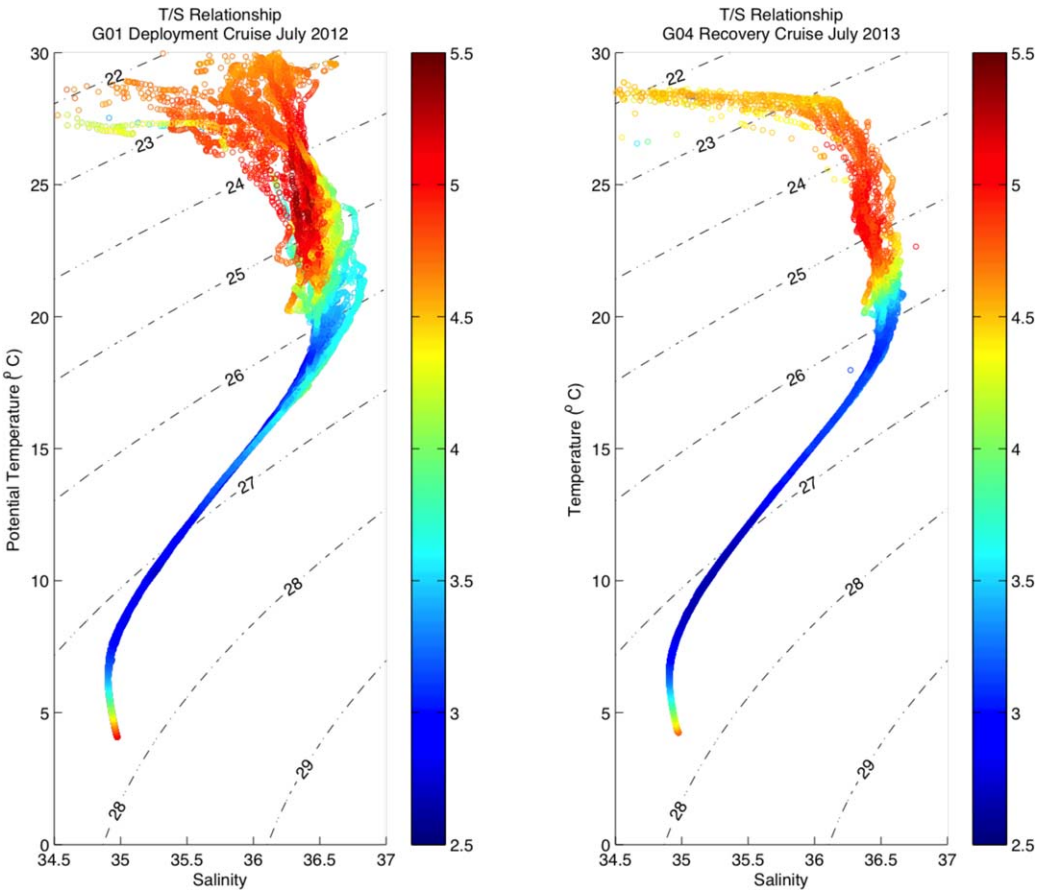

Figure 6. Temperature-salinity for CTD data. The temperature-salinity diagrams are shown for CTD data collected on G01 mooring deployment cruise in early July 2012 (left) and CTD data collected on G04 mooring recovery cruise in early July 2013 (right). The black contour lines show the isopycnals in kg/m^3. The colors represent dissolved oxygen concentrations.

stress curl was near zero before the storm and became positive as the hurricane approached before turning slightly negative after the passing of the storm. The right side of the hurricane track experienced the greater magnitude of wind stress curl than the left side during Hurricane Isaac. The estimate of wind stress near the moorings is used to determine descriptive parameters for Hurricane Isaac in Table 2. The evolution of the wind stress vectors during Isaac implies that the cyclonic wind stress curl from Hurricane Isaac likely induced the strong cyclonic current response observed in the current meter data.

3.5. Current Extremes

Before the approach of Hurricane Isaac, currents measured by Moorings 1–3 were flowing generally to the west, northeast, and south, respectively. As the hurricane approached, the measured top most flow changed simultaneously to strongly southwestward at each mooring. The maximum current speeds associated with Hurricane Isaac were observed at the shallowest recorded depths within 24 h of the storm's closest approach to the mooring array. The maximum current speed profiles for each mooring are shown in Figure 11. The top section of each plot shows the maximum recorded current speeds for each depth recorded by the ADCP for the entire yearlong record (dashed line), for the passage of the storm (thin line) defined as the period of time from 1 day before to 1 day after the storm, and the wake of the storm defined as the period of time from 1 to 14 days after the storm's closest approach to the mooring array on 28 September 2012 (bold line). The bottom section of each plot shows the maximum current speeds for each depth measured in the lower water column using the same identifying lines. Points are also included in the bottom section to show the depths of each measurement. Mooring 1 had the most observations in the lower water column with a total of six instruments deployed below the ADCP, while Mooring 2 lacked any

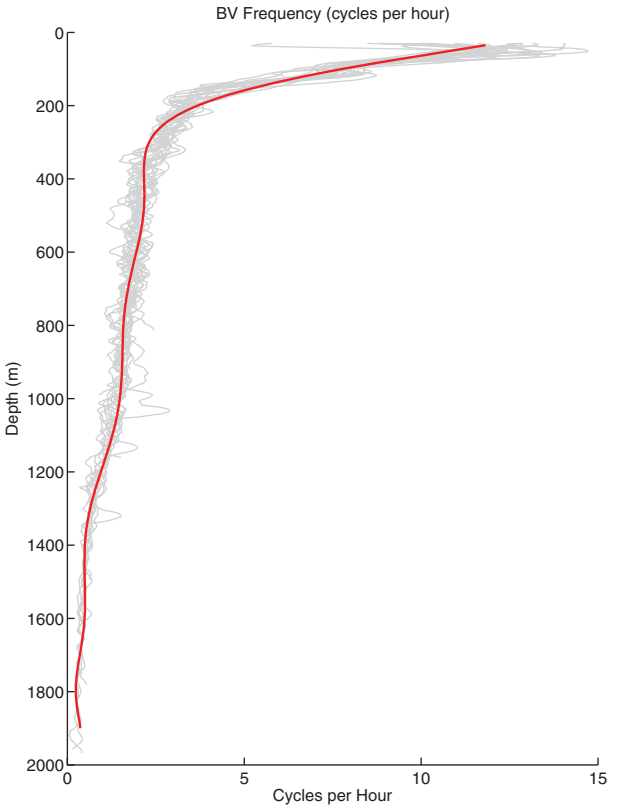

Figure 7. Brunt-Väisälä frequency Profiles. Brunt-Väisälä frequency profiles from CTD casts taken during the G01 mooring deployment cruise in July 2012. The gray lines represent each individual mooring's Brunt-Väisälä frequency profile, and the red line is the estimated best-fit profile used for calculations.

lower water column measurements due to the loss of instruments during recovery. The remaining moorings each featured three recording current meters (RCMs) that captured the lower water-column response.

Mooring 1, the mooring located nearest to the hurricane track, observed a maximum current speed of 50 cm/s at the shallowest recorded depth of 86 m within 24 h of the storm's closest approach. With the exception of Mooring 1 and the near-surface records (above 100 m), the maximum current speeds associated with Hurricane Isaac were observed days later in the storm's wake, not during the passage of the storm. All moorings also observed stronger near-bottom currents speeds during the wake of Hurricane Isaac compared to when the storm passed over the mooring. Figure 11 shows that the near-bottom speeds recorded during the wake of Hurricane Isaac were the maximum speeds observed during the yearlong records, but at all other depths the maximum current speeds were not observed during the passage or the wake of Hurricane Isaac.

3.6. Near-Inertial and Subinertial Response

In addition to high currents speeds observed during the wake of Hurricane Isaac, spectral and wavelet analysis shows a strong near-inertial oscillation (Figure 12) and two subinertial oscillations with periods of 2–5 days (Figure 16) and 5–12 days (Figure 18) are observed in each of the mooring velocity records. All moorings showed a strong increase in variance in the near-inertial band in the upper water column, but not all moorings experienced the same degree of variance in each subinertial band. Spectra for the u and v velocity components for Moorings 2 and 4 (Figure 12) show a peak in variance in the range of periods between 5 and 12 days. The variance is generally larger for shallower depth levels at each mooring. Table 3 shows the depth averaged variance percentages for the year record and the Hurricane Isaac period for each velocity component from each ADCP in the near-inertial band, the first subinertial band and the second subinertial band, respectively. The moorings located nearest the hurricane track (M1, M2, and M4) experienced the maximum increase in variance in the near-inertial band at shallower depths (less than 150 m). Moorings 3–6

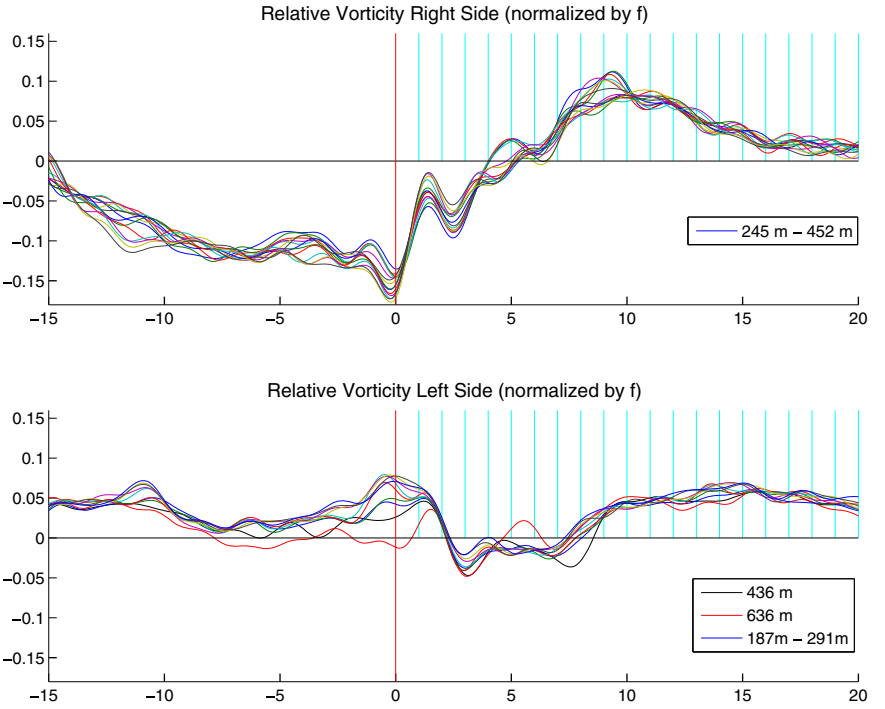

Figure 8. Normalized vertical component of relative vorticity time series. Vertical relative vorticity normalized by Coriolis parameter f on the left and right sides of the Hurricane Isaac storm track between −15 inertial periods and 20 inertial periods. The red vertical line represents the closest approach of Hurricane Isaac. The vertical blue lines are at intervals of one inertial period. The right side relative vorticity is estimated from ADCP time series records between 245 and 452 m at Moorings 1–3. The left side relative vorticity is estimated from ADCP time series records between 187 and 291 m and RCM records at 436 and 636 m at Moorings 1, 4, and 6. All relative vorticity is computed from 40 HRLP velocities.

all experienced maximum increases in variance associated with the near-inertial band much deeper in the water column (between 700 and 900 m).

The variance associated with the SUB1 and SUB2 bands (Table 3) generally increased during the storm at all moorings except Mooring 3 in SUB2 band. Mooring 2 observed the greatest increase in variance associated with the SUB1 band (Table 3), over 25% of the total variance in the u velocity component, while the other moorings experienced only small increases in variance (15% or less of total variance during the storm period). The SUB2 band observed consistently greater percentages of variance associated with the passage of Hurricane Isaac with the exception of Mooring 3, where there was a decrease in variance (40–70% decrease) associated with the SUB2 band during the period of the storm (Table 3). Mooring 4 measured the greatest amount in variance (over 25%) in both the u and v velocity components associated with the SUB2 band between 150 and 200 m. Mooring 6 also observed higher amounts of variance in u velocity component variance percentage (over 25%) near 800 m associated with the SUB2 band. Mooring 2 observed a high amount of variance of nearly 20% above 100 m in the u velocity component record associated with the SUB2 band (Table 3).

3.7. Near-Inertial Response

A wake of near-inertial internal waves was observed at all moorings after Hurricane Isaac passed over the GISR mooring array on 28 August 2012 (Figure 13). The strong near-inertial oscillations are observed immediately after the passage of the storm and persist for approximately 10–15 days (Figure 13). The propagation of near-inertial energy into the water column is apparent in Moorings 1, 3, and 4 while near-inertial energy is trapped near the surface at Mooring 2. Wavelet analysis performed on the current meter records revealed an increase in the effective frequency of the near-inertial band after the passage of Hurricane Isaac. An increase in the near-inertial band frequency was observed in the band pass filtered velocity records from all moorings (Figure 13). The frequency shift began approximately two inertial periods after the storm and lasted for about five inertial periods (Figure 14). Wavelet analysis was performed on the current meter

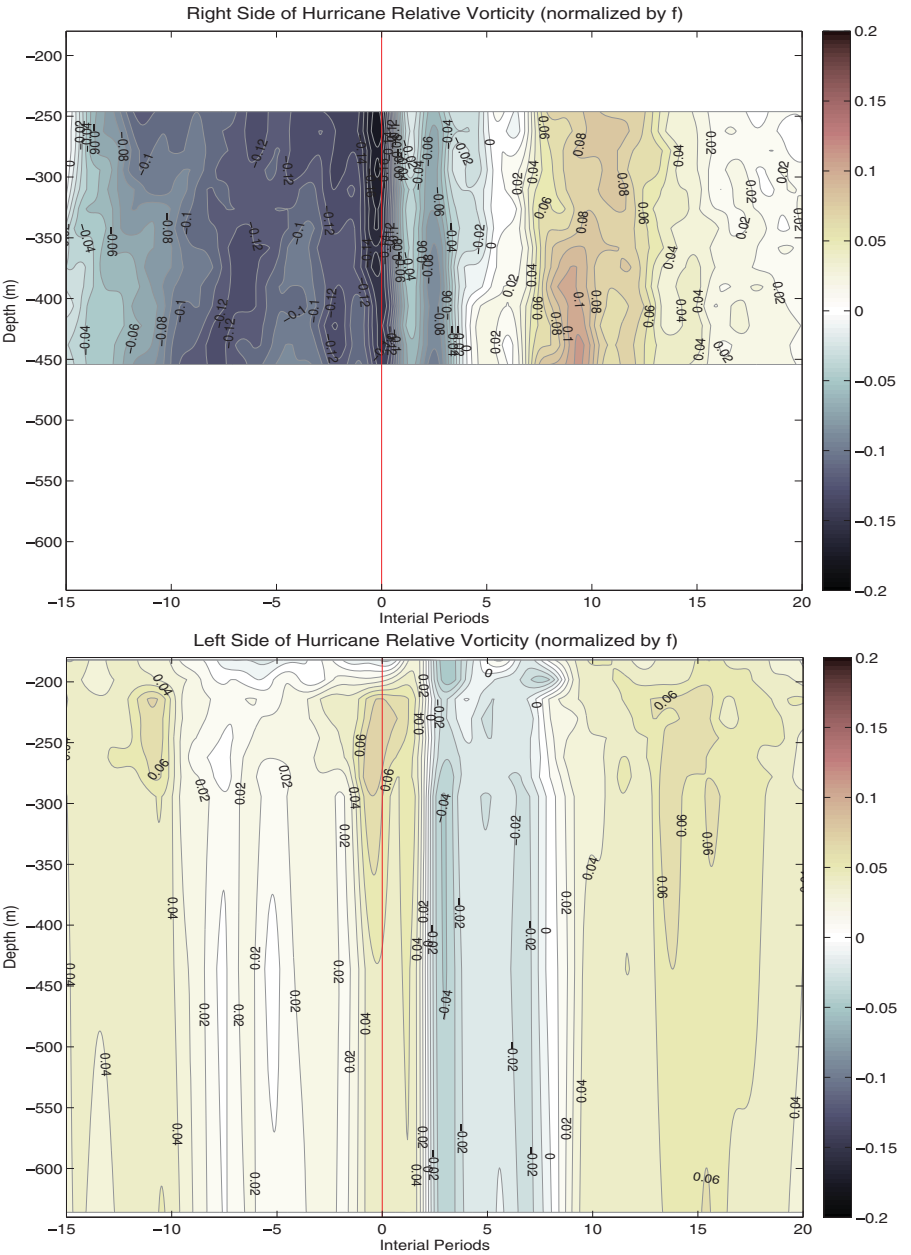

Figure 9. Normalized vertical relative vorticity contours. Vertical relative vorticity contours normalized by Coriolis parameter f on the left and right sides of the Hurricane Isaac storm track between −15 inertial periods and 20 inertial periods. The red vertical line represents the closest approach of Hurricane Isaac. The right side relative vorticity is estimated from ADCP time series records between 245 and 452 m at Moorings 1–3. The left side relative vorticity is estimated from ADCP time series records between 187 and 291 m and RCM records at 436 and 636 m at Moorings 1, 4, and 6.

records captured by the ADCP at Mooring 1, and then the resulting output was partitioned between two and seven inertial periods after the storm to isolate the storm's wake and highlight the shift in frequency. Figure 14 shows the frequency shift observed at Mooring 1 from two to seven inertial periods after the storm at every other ADCP depth level using a product of wavelet analysis. Each partition was plotted below the previous depth level in order to show how the inertial frequency changed throughout the water column in the wake of the storm. Warmer colors (reds) represent greater variance, while the cooler colors (blues) represent less variance. The strongest amounts of variance are observed higher in the water column at 118 m as seen in Figure 14. Also, there is a shift of the highest level of variance to a lower period (higher frequency) in the wake of Hurricane Isaac. The analysis shows that this observed near-inertial frequency was

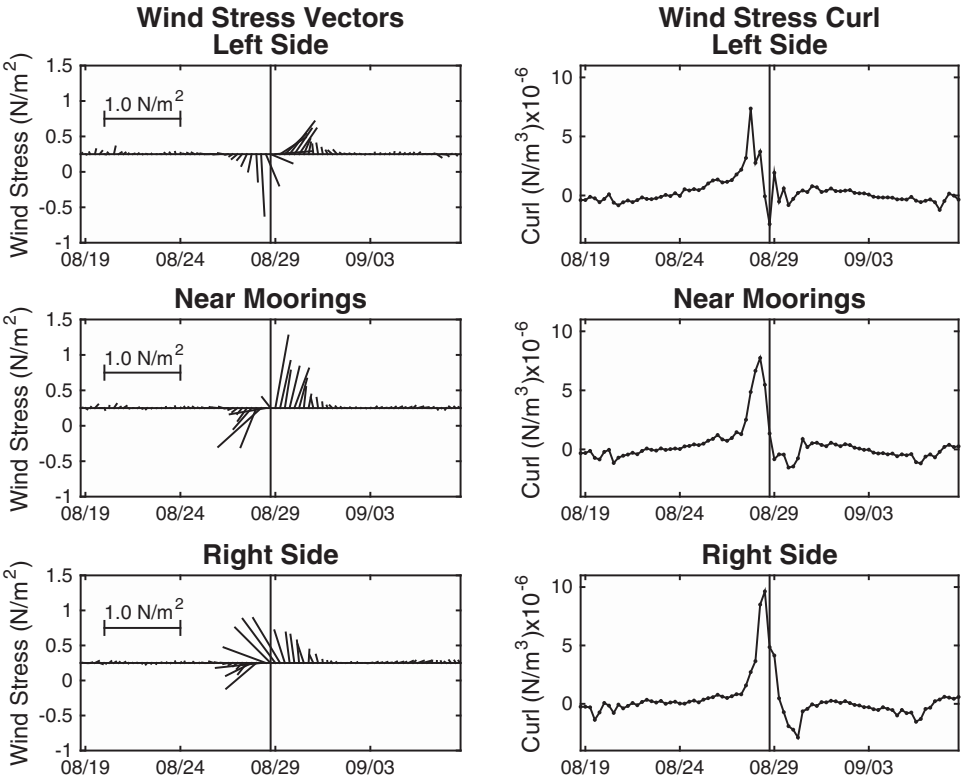

Figure 10. Wind stress and vertical component of the wind stress curl. Wind stress vectors and wind stress curl time series for sites near the mooring array, to the left of the storm track, and to the right of the storm track as shown in Figure 8. The stick plots in the left column represent the direction and speed of the wind near the time of Hurricane Isaac, with vertical lines corresponding to north and south, and horizontal lines corresponding to east and west directions. In the right column of plots, each window shows the wind stress curl at each location. The vertical line indicated the passage of Hurricane Isaac. Dates are in UTC.

generally less than the local Coriolis frequency at each mooring location, indicating a "blue shift" in frequency. The average effective frequency observed at each mooring was 1.11*f* with *f* being the local Coriolis frequency. A similar blue shift in frequency was observed in response to Hurricane Isaac at all other moorings. We will have more discussions on the causes of the "blue shift" in the next section.

3.7.1. Phase Shift

The deployment depths of each mooring limited the amount of velocity data available from the upper water column. Only Moorings 1, 2, and 4 measured velocity data above 100 m with the shallowest recorded depths being 86 m at Mooring 1, 52 m at Mooring 2, and 35 m at Mooring 4. At Moorings 2 and 4, there was a phase difference observed between the mixed layer and the upper thermocline where leading phases with increasing depth. Mooring 2 had near-inertial energy trapped in the mixed layer, above 100 m. The depth of near-inertial energy at Mooring 4 was initially be much deeper in the water column, ~150 m, and a depth-leading phase appears within two inertial periods after the passage of Hurricane Isaac. Mooring 1 also experienced a depth-leading phase with higher amplitudes beginning after two inertial periods of the storm's passage. Moorings 1 and 3 showed coherent vertical phase distributions profiles, with a gradual decrease in phase with increasing depth (3 h phase lead at 198 m compared to 86 m at Mooring 1). This positive tilt in the phase distribution with depth is indicative of downward propagation of energy into the thermocline.

Comparison between similar depth levels between moorings using wavelet coherence analysis confirms the propagation direction of the near-inertial energy was away from the storm path. Moorings 1 and 3 are aligned perpendicular to the hurricane track with Mooring 1 being closest to the storm path. The wavelet coherence analysis further reveals that the two records are strongly coherent and nearly in phase in the near-inertial band, with the phase of Mooring 3 leading Mooring 1. This small phase lead indicates propagation of near-inertial energy from Mooring 1 to Mooring 3, or away from the hurricane track.

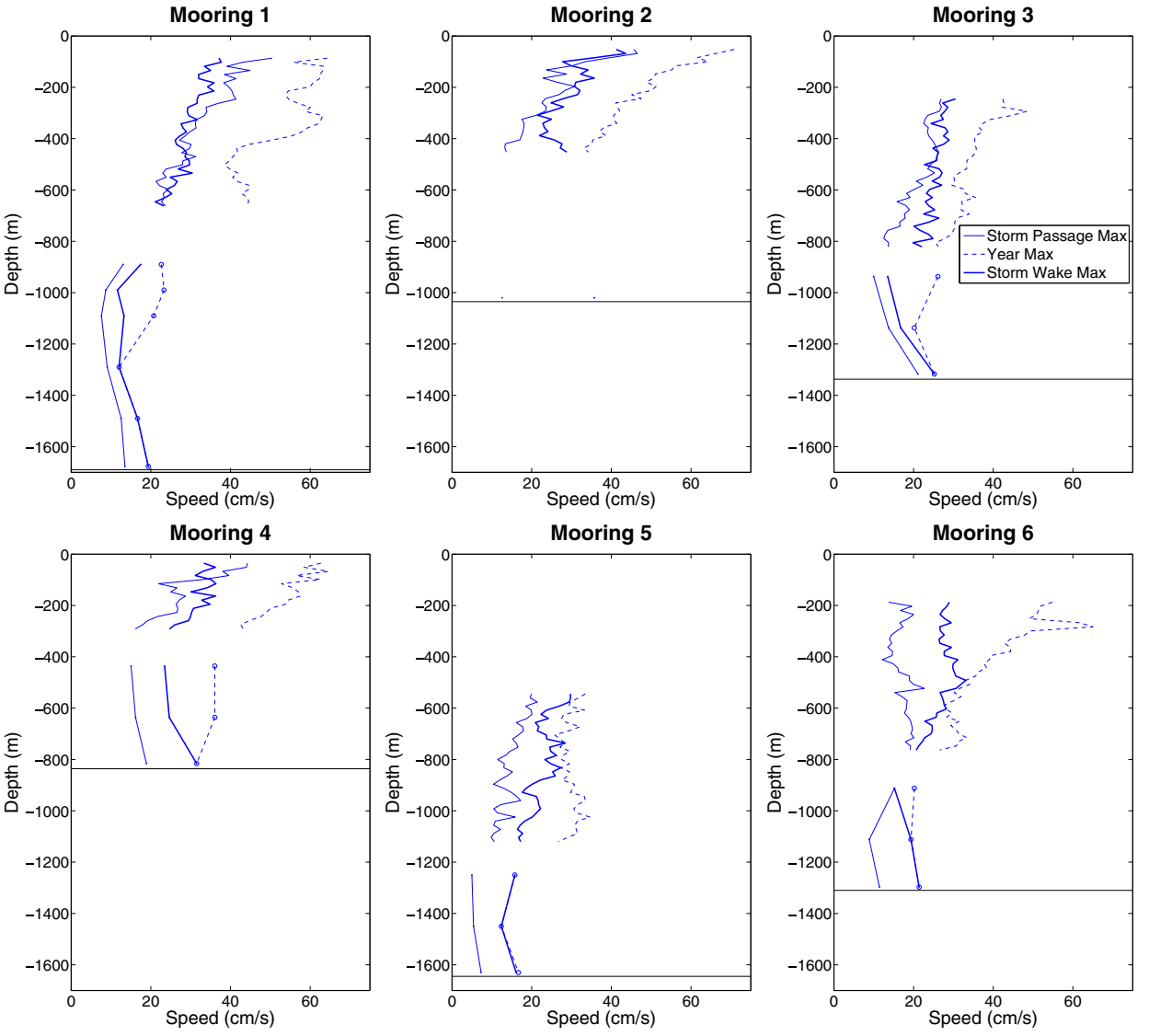

Figure 11. Maximum current speed profiles. Maximum current speeds for Hurricane Isaac during the period of the storm (thin straight line), in the wake of the storm (bold straight line), and for the yearlong time series (dashed line). The top section of each plot shows the ADCP data and the bottom section shows the RCM and S4A data, all at their corresponding depths. The statistics were calculated from the quality controlled unfiltered velocity data. The storm wake refers to the period 1 to 14 days after the time of the storm's closest approach to the mooring array at 18:00 UTC 28 August 2012. The time period for the passage of the storm is from 27 August 2012 18:00 (1 day before the storm arrival) to 29 August 2012 18:00 (1 day after the storm arrival).

3.7.2. Vertical Scale

The phase difference of 3 h between the shallowest depth at Mooring 1 (86 m) and the thermocline depth (198 m) indicates a vertical scale of approximately 845 m after three inertial periods following the storm. This is greater than the thermocline thickness, but less than the total water depth. After five inertial periods after the storm, the phase lead with depth increased to 4 h, indicating a new vertical scale of 633 m.

A phase difference of 1 h was observed between the mixed layer at Mooring 4 (35 m) and the upper thermocline (86 m) just three inertial periods past the storm's passage. This indicated a vertical scale of approximately 1086 m. The phase difference increased to a 3 h phase lead in the upper thermocline five inertial periods after the storm, indicating a much smaller vertical scale of 362 m. The estimated vertical scale for the near-inertial response will be 965 m, the average of the

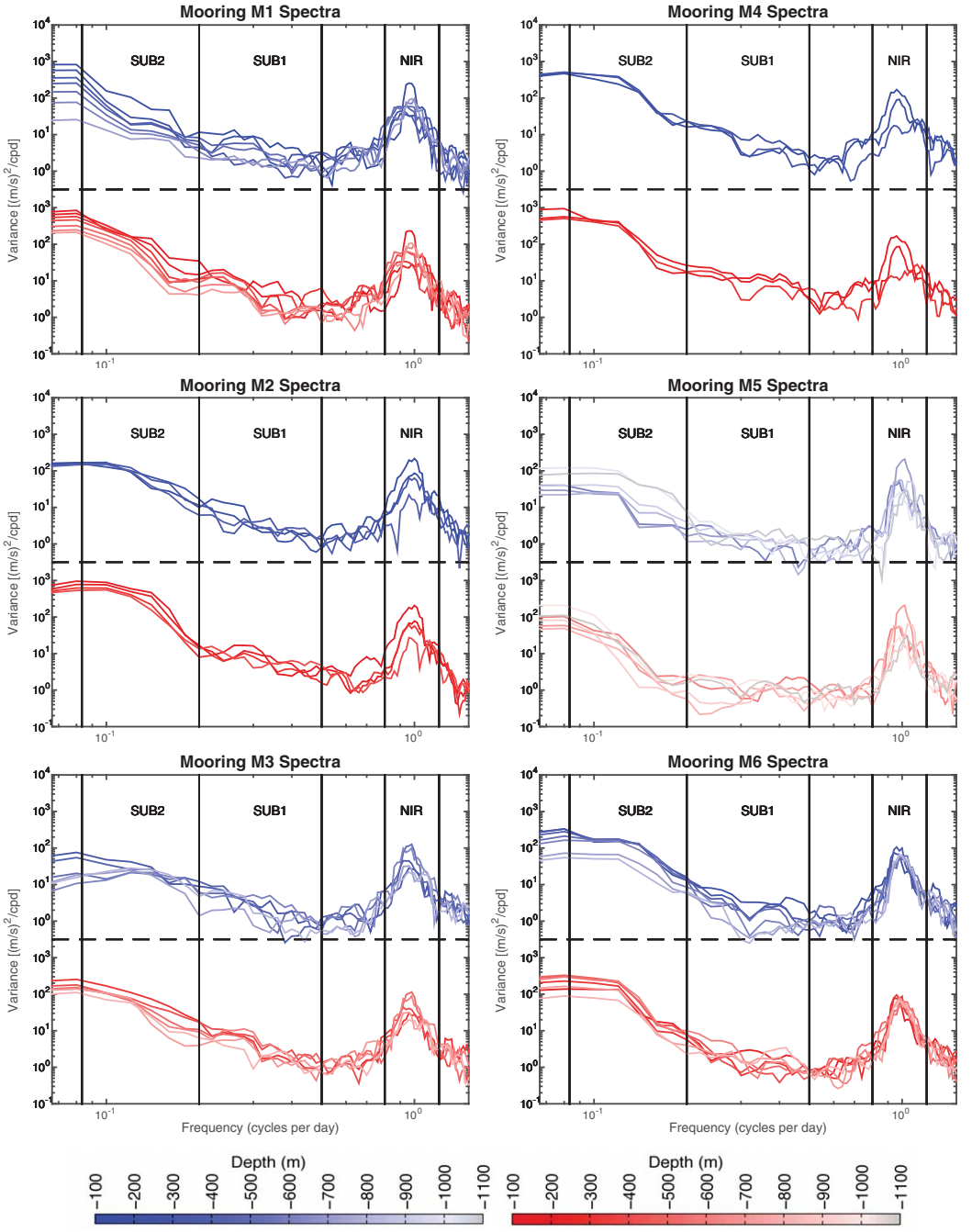

Figure 12. Spectra for ADCP data. Spectra for velocity components u (red) and v (blue) for each 100 m depth level available from each ADCP. Darker colors correspond to shallower depths. Black vertical lines in each figure correspond to frequency intervals (NIR band: 0.8f–1.2f, SUB1 band: 2–5 days, and SUB2 band: 5–12 days). Velocity records were analyzed for the time interval from 42 days before the storm and 85 days after the storm.

Moorings 1 and 4 vertical scales. The corresponding vertical wavenumber for the near-inertial response is estimated to be 0.03 km^{-1}.

Between four and five inertial periods after the storm, both Moorings 1 and 4 experience an amplitude minimum in the depths between 100 and 200 m. The maximum phase difference measured between the mixed layer (52 m) and the upper thermocline (100 m) at Mooring 2 was 9 h, indicating a vertical scale of only 120 m. At Mooring 2, the near-inertial energy was trapped in the mixed layer and unable to penetrate into the thermocline.

Table 3. ADCP Variance Table[a]

Mooring	Velocity Component	Depth Avg Variance % Year	Depth Avg Variance % Storm	Max Variance % Storm	Max Variance % Depth (m)
NIR Band					
1	*u*	9.1	26.9	58.8	86.2
	v	17.3	18.5	44.6	86.2
2	*u*	7.2	22.1	47.3	84.2
	v	10.1	25.4	54.5	68.2
3	*u*	11.1	36.4	53.1	741.2
	v	16.4	21.5	46.5	757.2
4	*u*	9.9	26.5	49.5	67.2
	v	11.6	32.3	75.1	67.2
5	*u*	23.3	33.1	55.4	848.2
	v	23.0	24.5	35.9	848.2
6	*u*	15.2	22.4	38.5	699.2
	v	13.9	25.7	45.2	699.2
SUB1 Band					
1	*u*	1.1	3.1	6.4	150.2
	v	3.0	4.0	6.8	214.2
2	*u*	3.0	17.7	28.0	132.2
	v	4.0	7.3	15.9	116.2
3	*u*	1.8	5.1	8.1	357.2
	v	3.0	2.2	3.7	629.2
4	*u*	2.8	7.0	11.0	259.2
	v	2.9	7.3	11.7	147.2
5	*u*	2.0	6.3	9.9	768.2
	v	2.1	4.1	7.3	976.2
6	*u*	1.8	4.6	9.4	763.2
	v	1.4	5.9	14.1	395.2
SUB2 Band					
1	*u*	4.3	10.0	17.5	214.2
	v	7.4	9.6	12.8	614.2
2	*u*	6.6	8.0	19.2	52.2
	v	8.0	7.4	11.1	132.2
3	*u*	5.8	3.4	5.3	453.2
	v	12.0	3.8	7.8	821.2
4	*u*	6.5	18.5	26.9	195.2
	v	8.4	21.3	31.5	179.2
5	*u*	4.9	6.1	13.8	928.2
	v	5.0	14.1	19.6	1104.2
6	*u*	4.8	14.1	26.5	747.2
	v	5.3	10.1	15.3	747.2

[a]Tables of depth averaged variance percentages for each ADCP velocity component data for the yearlong record and the Hurricane Isaac storm period. The storm period variance was calculated for velocity records between 18 August 2012 and 12 September 2012.

3.7.3. Horizontal Scale

A horizontal cross-track scale of 176–235 km was calculated from the observed phase difference of 3–4 h between the rotated u-velocity records at Moorings 1 and 3 near 300 m. The 176 km horizontal along-track scale was calculated at the same time period from the phase differences of 4 h between the rotated v-velocity records at Moorings 1 and 2 at 200 m. The estimated horizontal scale for the near-inertial response will be 205 km, the average of the scale determined between Moorings 1 and 3 and between Moorings 1 and 2. The horizontal wavenumber for the near-inertial response will be 6.6 km^{-1}.

The phase angle calculated from the spatial scales is tan $\theta = 0.004$ (0.27°), compared with the tan $\theta = 0.007$ (0.44°) estimation from the dispersion relation.

The estimated horizontal and vertical group velocities were calculated using the average vertical and horizontal wavenumbers (l, m) = (0.03, 6.61 km^{-1}) and the estimated Brunt-Väisälä frequency of 3.7 cycles/h. The horizontal group velocity (C_{gy}) was approximately 5.7 km/d and the vertical group velocity (C_{gz}) was approximately 29 m/d into the water column calculated from equations (5a) and (5b) [*Brooks*, 1983].

The downward propagation of energy in the near-inertial band is also observed in the wavelet analysis of the current meter records from the ADCPs. Figure 15 shows the scale average of variance of the north-south velocity component at each depth for each ADCP location. The scale average of variance for each

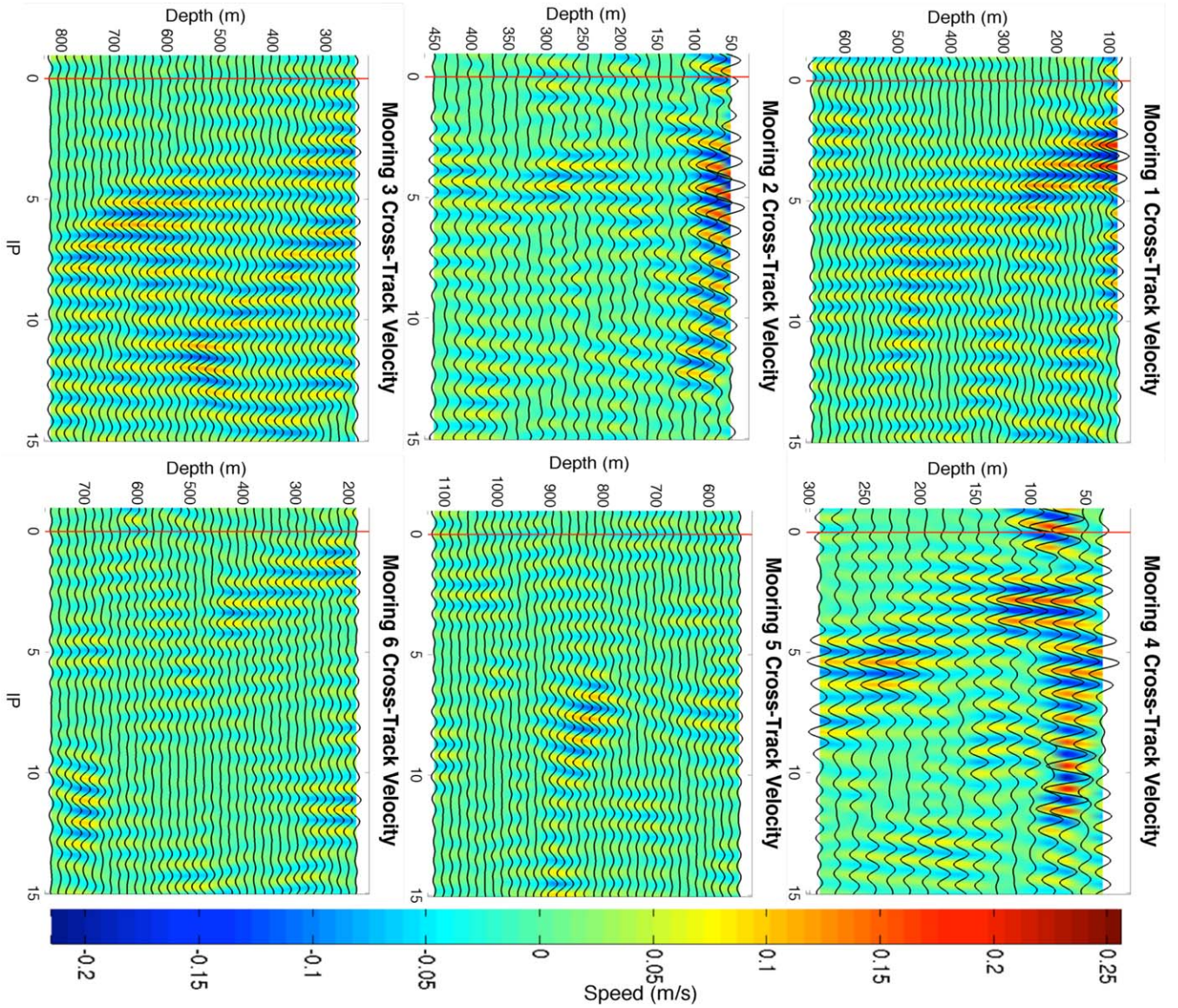

Figure 13. Cross-track component of velocity measured from ADCP at each mooring location from one inertial period before the storm to 15 inertial periods after the storm. The red vertical line refers to the time of the closest approach of Hurricane Isaac. The background contour in each plot refers to the amplitude of the measured velocity in m/s. The near-inertial band-passed record for each available depth from the ADCP is overlaid at the corresponding depth. Notice that the depth ranges of each figure vary according to the depth of the ADCP. Moorings 2 and 4 have fewer depth levels due to their shallow deployment depths.

time series is a vertical integration of the wavelet power spectrum of the periods between 12 and 36 h. The integrated values are obtained for each depth level to show the time and space evolution of variance within the NIR (near-inertial) band at each mooring. Figure 15 shows the confinement of near-inertial energy in the mixed layer at Mooring 2 and the propagation of energy into the thermocline at Moorings 1 and 3. The color scales are independent between each mooring in order to better show the propagation of energy into the water column.

3.8. Subinertial Response

In addition to the strong near-inertial response in the wake of Hurricane Isaac, two elevated subinertial period bands were observed in the current meter spectra. One subinertial band (SUB1) is characterized by a 2–5 days period (0.5–0.2 cpd frequency) and featured maximum speeds associated with this band of over 16 cm/s (Figures 16 and 17). The second subinertial band (SUB2) had a longer period between 5 and 12

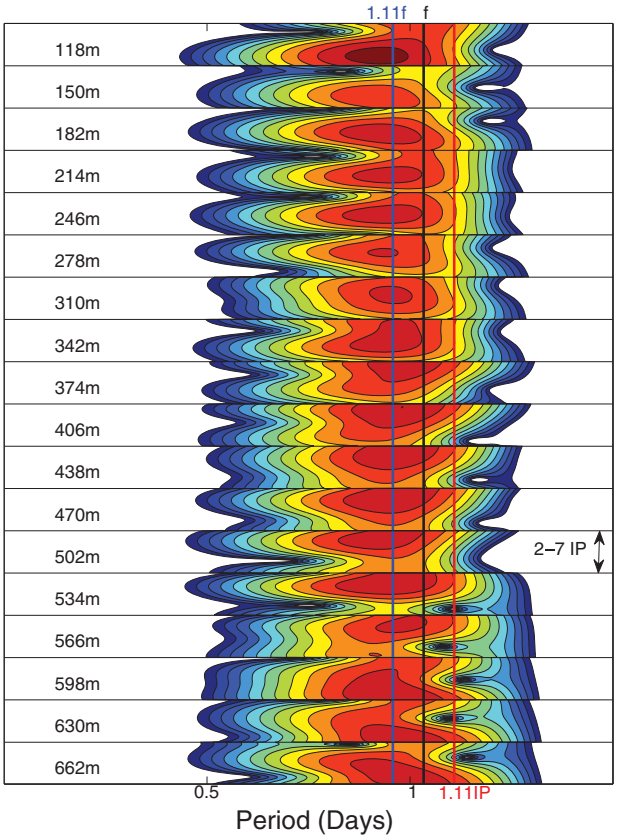

Figure 14. Frequency shift at Mooring 1. Mooring 1 near-inertial partitioned wavelets at depths captured by the ADCP show the blue shift in frequency in the wake of Hurricane Isaac. Each slice represents the 2–7 inertial period partition of the wavelet of the current meter record from the each depth. The black line is the local inertial period, or $2\pi/f$, at Mooring 1. The blue line is $2\pi/(1.11f)$, representing the average blue shift in frequency observed in the wake of the storm. The red line represents 1.11 IP, or $2\pi/(0.9f)$, which would be a red shift in frequency. Warmer colors represent higher variance observed at the corresponding period.

days (0.08–0.2 cpd frequency) and expressed a smaller degree of speed, 12.5 cm/s maximum at Mooring 4 (Figures 18 and 19), but accounted for a higher percentage of the total variance observed in the current meter records as seen in Table 3. The current responses at all moorings and in each subinertial band show a strong barotropic response that is observed throughout the water column and varies in intensity between each mooring. This strong barotropic response is fundamentally different than the near-inertial response. The subinertial response is simultaneous throughout the water column, whereas the near-inertial response propagates downward through the water column.

Horizontal wavelengths and propagation speeds for these subinertial waves could not be calculated due to the inconsistent observations of these waves between the moorings. Despite the close proximity of the moorings to the hurricane track, the records did not show coherence phase between moorings. Also, the arrangement of the moorings in the water column did not allow for acceptable reliable estimations of horizontal speeds. Wavelet coherence analysis on the velocity records show strong coherency ($<$0.8) in both subinertial bands during the passage of Hurricane Isaac, but no consistent direction of propagation could be determined. The lack of evidence to support propagation of the subinertial waves is also consistent with a nonpropagating barotropic response. The strong vertical coherence observed between depth levels at each mooring suggests the subinertial responses were forced by the passage of Hurricane Isaac.

3.8.1. 2–5 Days Band

The SUB1 featured the maximum speeds associated with this band at Mooring 2. The maximum speeds measured 17 cm/s and were observed in the upper 100 m of the water column at Mooring 2. The SUB1 response began before the closest approach of Hurricane Isaac to the mooring array (red vertical line in Figure 16) and last for a total of three to five oscillations or approximately 5–7 days after the passage of the storm. Each moorings observed a bottom intensified response in the RCM data collected 20 m above the

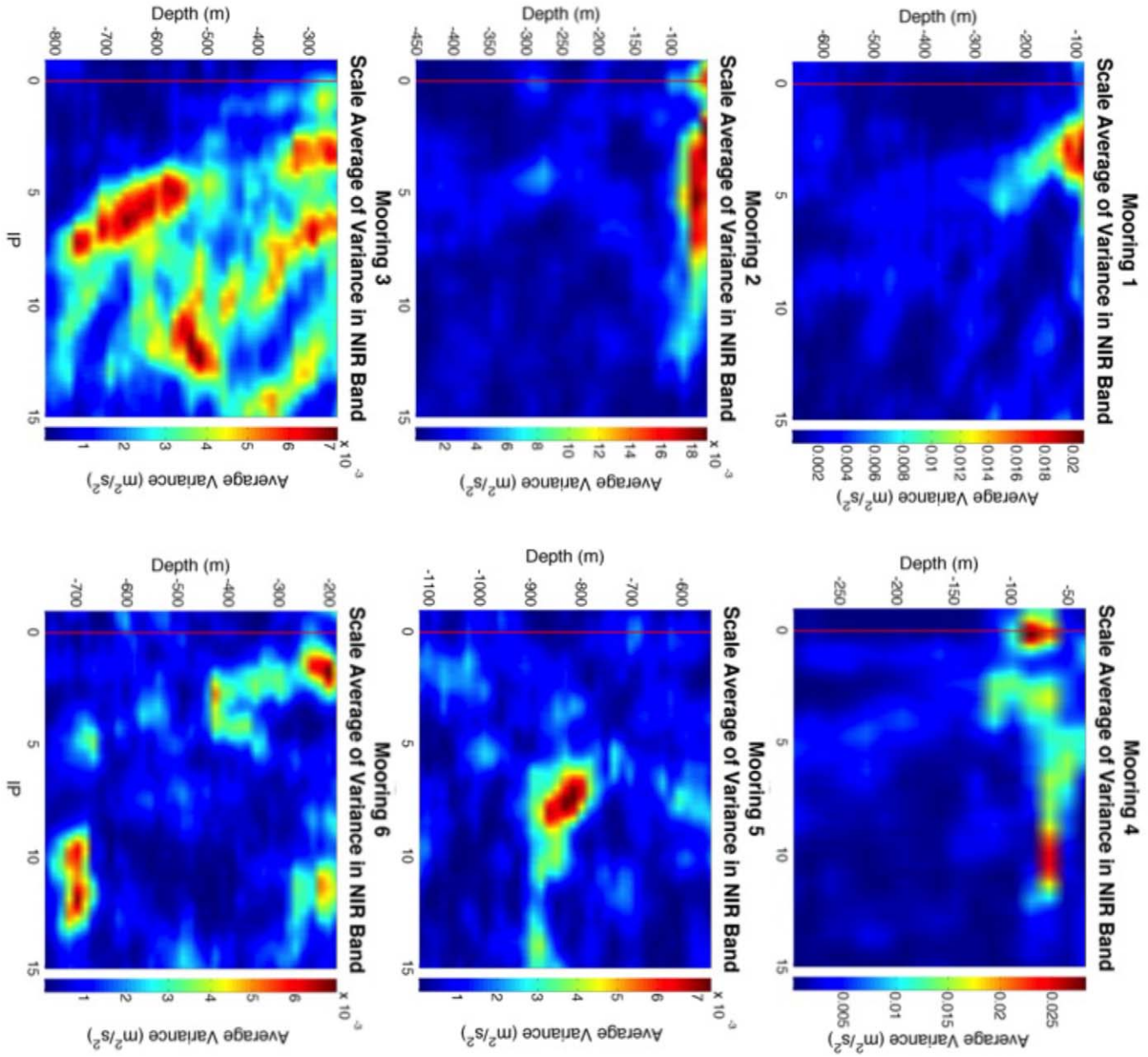

Figure 15. Scale average of variance in the NIR Band. Scale average of variance in the north-south velocity component measured from the ADCP at each mooring location from one inertial period before the storm to 15 inertial periods after the storm. The red vertical line refers to the time of the closest approach of Hurricane Isaac. The background color in each plot refers to the amount of variance measured at the corresponding time and depth level. The color scales are independent for each mooring.

ocean floor. The full water column profile for each mooring suggests bottom intensification with a gradual decrease in amplitude with decreasing depth. Mooring 4 was the only mooring to observe a strong phase shift between the shallowest record and the deeper current meter records. The shallow moorings (M2 and M4) experienced the maximum current response in the 2–5 days subinertial band compared to the deeper moorings. Figure 17 shows the wavelet products of scale average of variance in the 2–5 day subinertial response to Hurricane Isaac. The response was much greater at Moorings 2 and 4 compared to the deeper moorings, therefore the color scales differ between panels. Each figure shows the overlay of the depth anomaly time series derived from the pressure recorded at each ADCP instrument. The depth anomaly records are also band passed for the 2–5 days period and plotted at the depth level at which they were recorded. Mooring 2 observed the maximum depth anomaly of over 30 cm associated with the 2–5 days period band in the wake of Hurricane Isaac.

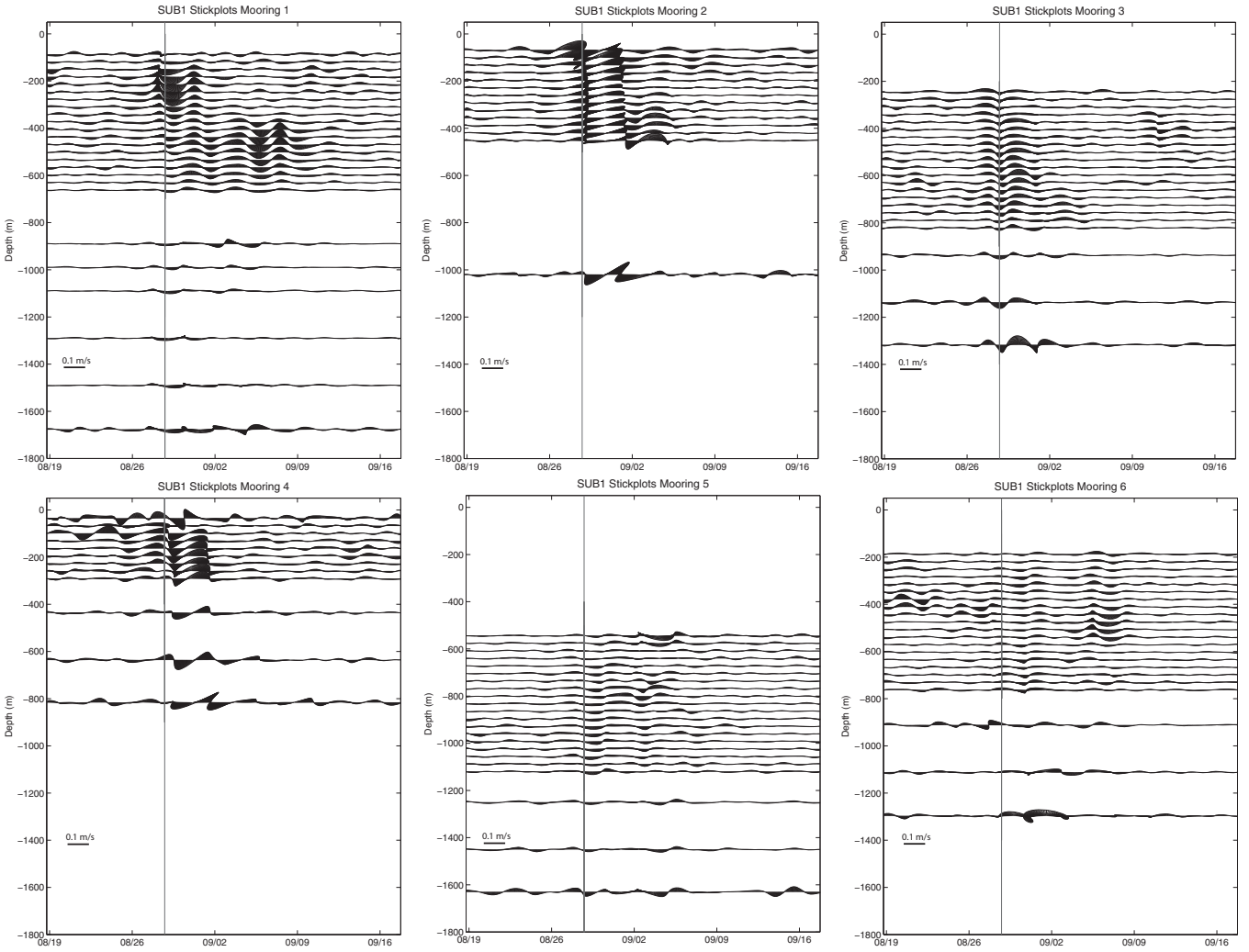

Figure 16. 2–5 day band velocity vector plots. Velocity vector plots for 2–5 day period current meter data at each mooring 10 days before and 20 days after the passage of Hurricane Isaac are shown. The vertical red line represents the closest approach of Hurricane Isaac on 28 August 2012 at 18:00 UTC. The direction of the vectors is oceanographic convention with currents pointing up on the page referring to currents coming from the south and flowing north.

3.8.2. 5–12 Days Band

The SUB2 featured a relatively large percentage of the total variance in the current meter records associated with Hurricane Isaac (Table 3). Increases in speed and variance in this band are observed intermittently throughout the current meter records, but there is a consistent increase in speed observed during and after the passage of Hurricane Isaac at most of the mooring sites. Figure 18 shows that Moorings 2 and 4 observed the strongest speeds in this band with Mooring 4 experiencing maximum speeds of 11.1 cm/s near 200 m and Mooring 2 experiencing maximum speeds near 11.5 cm/s above 100 m. At Mooring 2, all observations of speeds greater than 10 cm/s were found in water depths less than 100 m. In contrast, maximum speeds at Mooring 4 were observed at depths of 300 m, which is the deepest the ADCP measured. Mooring 1 also observed a full water-column north and south surging pattern in the velocity records (Figure 18), yet maximum speeds recorded were less than 9 cm/s. As with the SUB1 band, the response to Hurricane Isaac in the SUB2 band began before the arrival of the storm and persisted for approximately 7–10 days after the passage of the storm.

The SUB2 band response is bottom intensified only at Moorings 2 and 5, while surface intensification is observed at Moorings 1–4. As seen in the SUB1 band, Moorings 2 and 4 experienced a greater response in the SUB2 band associated with Hurricane Isaac. Figure 19 shows the wavelet products for the SUB2

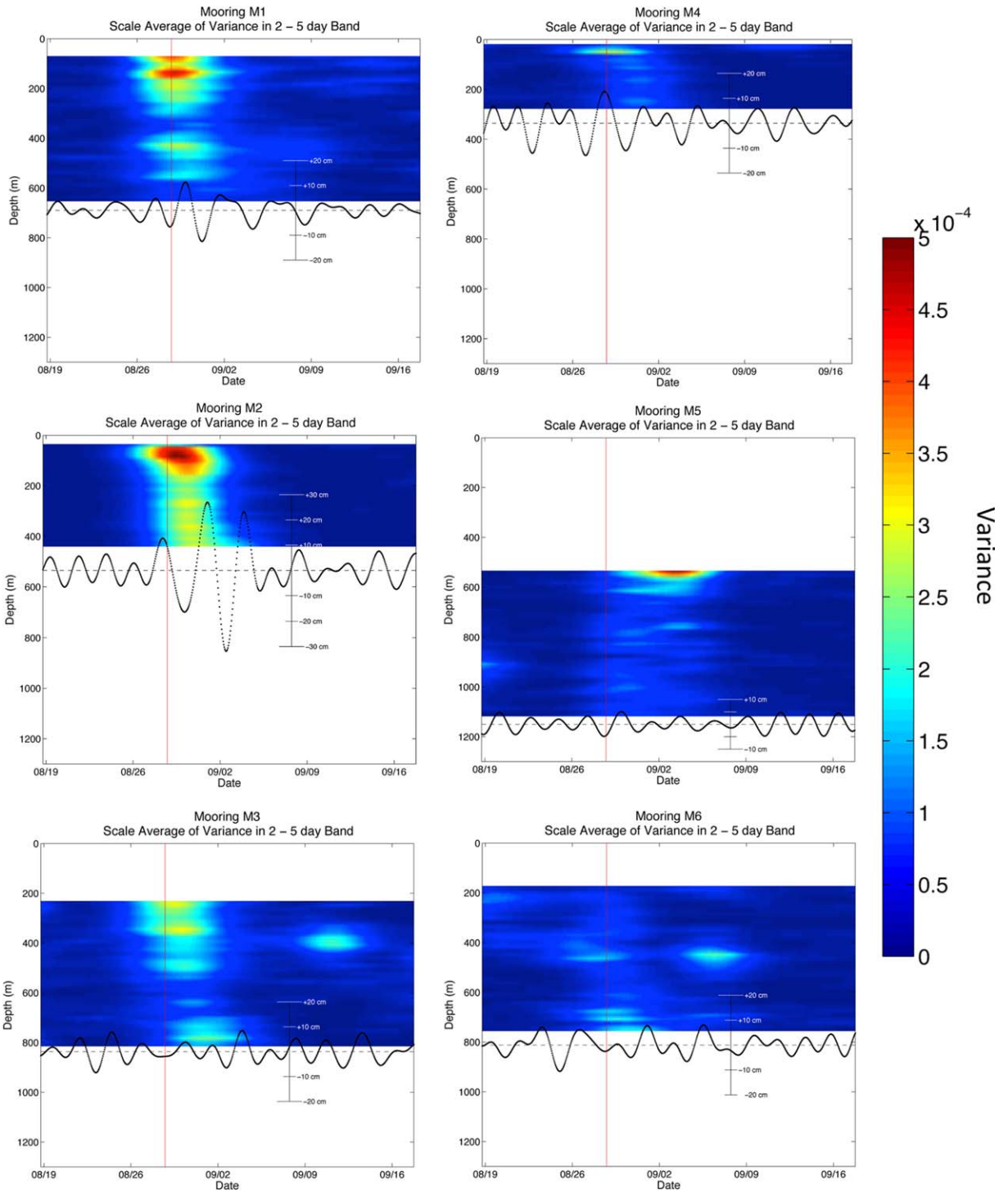

Figure 17. Scale average of variance for Mooring 2 (a) and Mooring 4 (b) in the SUB1 band from the east-west velocity component measured from the ADCP with overlay of the depth anomaly is shown. Scale average of variance in the 2–5 Day band at Moorings (c) 1, (d) 3, (e) 5, and (f) 6. The red vertical line references the time of the closest approach of Hurricane Isaac to the mooring array on 28 September 2012 at 18:00 UTC. The depth anomaly derived from pressure data is shown as black dots in each figure. The black dashed line shows the deployment depth of the ADCP instrument. Notice that the variance scale is different from Figures 17a and 17b.

response observed in each of the ADCP records. Mooring 2 experienced the largest amount of variance in the near-surface region of the water column associated with the SUB2 band. Although there is an increase in variance during the passage of Hurricane Isaac and in the storm's wake, energy in the SUB2 band is observed intermittently through the entire record.

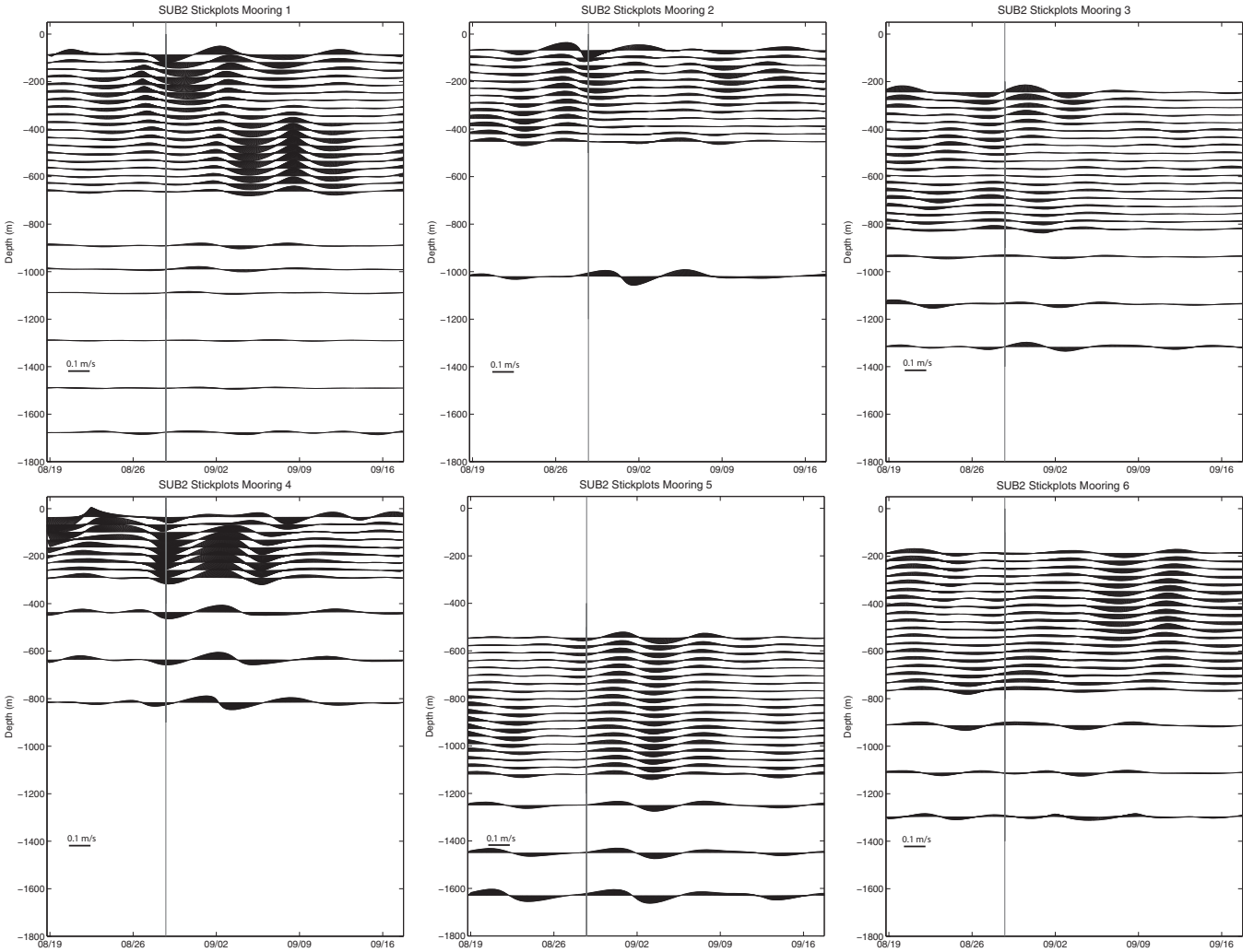

Figure 18. 5–12 day band velocity vector plots. Velocity vector plots for 5–12 day period current meter data at each mooring 10 days before and 20 days after the passage of Hurricane Isaac are shown. The vertical red line represents the closest approach of Hurricane Isaac on 28 August 2012 at 18:00 UTC. The direction of the vectors is oceanographic convention with currents pointing up on the page referring to currents coming from the south and flowing north.

4. Discussion

4.1. Hurricane Isaac

The characterization and description of the full water column near-inertial and subinertial response to Hurricane Isaac is presented in this study. Parameters to describe Hurricane Isaac were derived and compared to other storms in the Gulf of Mexico and the Northern Hemisphere and presented in Table 2. Hurricane Isaac, a Category 1 storm, was the least intense storm listed in the comparison. The translation speed of Hurricane Isaac (3.83 m/s) was only faster than Hurricane Norbert's translation speed of 3.0 m/s when it struck the Baja California Peninsula in 1984. The nondimensional storm speed of Hurricane Isaac (0.47) was considerably less than the compared hurricanes, which ranged between 1.0 and 2.4. In addition to the slower speeds, Hurricane Isaac also has a significantly larger radius of maximum winds, or cross track scale of 96 km compared to the other hurricanes which ranged from 20 to 60 km. The estimated wind stress of Hurricane Isaac was only 1.35 N/m^2 compared with the other reported wind stress values between 4.0 and 6.7 N/m^2. The wind stress value for Hurricane Isaac was estimated from the gridded NOAA wind product and not directly measured from flight data as in the case of the other hurricanes presented. The maximum wind stress based on direct observations of maximum sustained wind of 36 m/s in the northern Gulf of Mexico during Isaac is 3.24 N/m^2 [*Berg*, 2013].

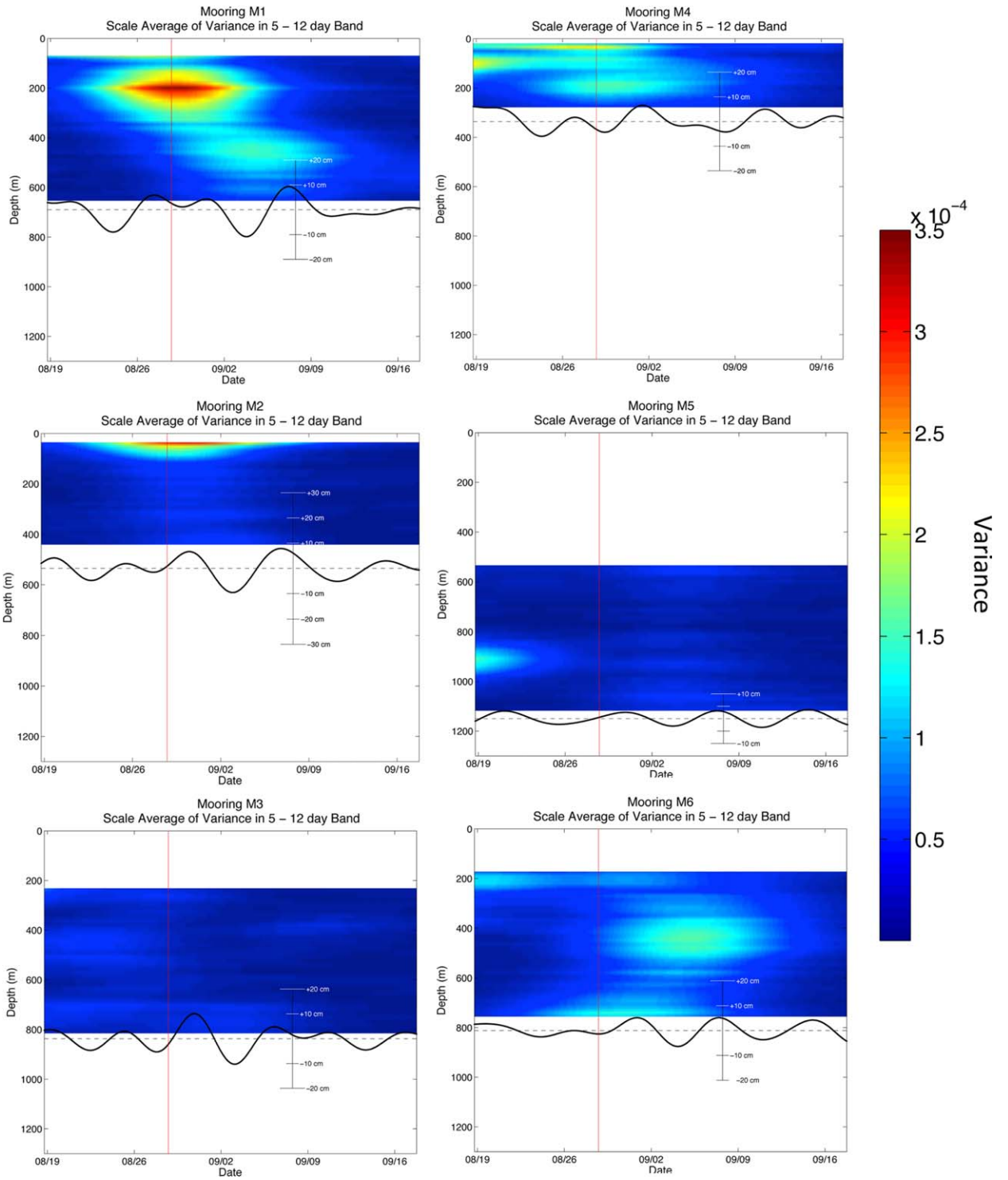

Figure 19. Scale average of variance for (a) Mooring 2 and (b) Mooring 4 in the SUB2 band from the east-west velocity component measured from the ADCP with overlay of the depth anomaly. Scale average of variance in the 5–12 day band at (c) Moorings 1, (d) 3, (e) 5, and (f) 6. The red vertical line references the time of the closest approach of Hurricane Isaac to the mooring array on 28 September 2012 at 18:00 UTC. The depth anomaly derived from pressure data is shown as black dots in each figure. The black dashed line shows the deployment depth of the ADCP instrument.

The Burger number B is a measure of the pressure coupling between the mixed layer current and the thermocline current. For Hurricane Isaac, B = 0.009 compared to the other storms which ranges between 0.006 and 0.37. The Burger number equation shows that the oscillations would be faster for smaller R_{max} or weaker stratification. The R_{max} for Hurricane Isaac was large compared to other storms, which is consistent with the Burger Number for Isaac being an order of magnitude less than other storms in the Gulf of Mexico and the eastern Pacific storm (Norbert), where stratification can be stronger. Although we further note that in the cases presented in Table 2, the dominate control on Burger is R_{max} as each of the five listed hurricanes have similar stratification as indicated by the similar reduced gravity estimates.

The maximum measured currents associated with Hurricane Isaac showed maximum current speeds were found near the surface and in the wake of the storm (Moorings 2 and 4 in Figure 8). Despite the intense event of the storm's passage, the maximum currents observed in the current meter records were not associated with the passing of Hurricane Isaac. This implies that energetic and persistent events, such as an eddy, likely impacted the mooring area, resulting in the maximum currents speeds observed throughout most of the water column.

4.2. Oceanic Response

The near-inertial and subinertial responses observed in the wake of Hurricane Isaac showed a difference between the left and right sides of the storm path. The maximum currents were greater on the right side of the storm path compared to the left side. This is consistent with previous studies that observed sea surface temperature differences on each side of the hurricane track that lead to the expectation of a rightward bias of the storm's current response [*Church et al*., 1989; *Sanford et al*., 1987; *Shay et al*., 1992, 1998]. More energetic near-inertial motions were present on the right side of the hurricane track as also observed in the study of Hurricane Ivan [*Teague et al*., 2007]. The left and right sides of the storm path also observed differences in the response of relative vorticity to the hurricane passage. The passage of Hurricane Isaac, a strong cyclonic force, added positive relative vorticity to the mooring region as shown in Figures 8 and 9, but the increase in relative vorticity was not uniform on each side of the hurricane track. The right side of the storm path experienced a larger increase in relative vorticity compared to the left side. The wind stress values estimated for each side of the storm path also indicates a stronger response on the right side of the storm path compared to the left (Figure 10). Numerical ocean models have been used to explain that the directions of the wind stress vectors are responsible for the pronounced rightward bias of the response to a hurricane [*Bender et al*., 1993; *Price*, 1983].

In addition to the differences between currents observed on each side of the storm path, a noticeable difference was observed between the responses measured at the moorings deployed in shallower areas (less than 1050 m) and moorings deployed in deeper water (between 1300 and 1700 m), especially in the subinertial responses. The shallow mooring sites (Moorings 2 and 4) measured significantly larger amount of variance in the 2–5 and 5–12 days subinertial responses after Hurricane Isaac as shown in Figures 17 and 19. Less intense subinertial responses were observed at the deeper mooring sites. The more intense response at the shallower mooring sites could be explained by the influence of the continental shelf.

4.3. Near-Inertial Response

After the passage of Hurricane Isaac, a strong near-inertial response was observed in the current meter records. A large increase in variance in the near-inertial band was observed at all moorings. Moorings 1, 2, and 4 all experienced the maximum increases in variance in the upper part of the water column as expected. Moorings 3, 5, and 6 all experienced maximum increases in variance associated with the near-inertial band much deeper in the water column (between 700 and 900 m). This may be due to the deeper deployment of the moorings as with M5, or to the increased distance away from the hurricane track. The near-inertial response began immediately after the passage of the storm and persisted for approximately 10–15 days. This is similar to other observations of the near-inertial response to a hurricane in the Gulf of Mexico [*Brooks*, 1983; *Shay and Elsberry*, 1987; *Teague et al*., 2007].

The near-inertial response to Hurricane Isaac included the propagation of near-inertial energy away from the hurricane track and down to the thermocline over time. Moorings 1, 3, and 4 showed vertical propagation into the thermocline over time after the passage of Hurricane Isaac at a rate of approximately 29 m/d. Horizontal propagation speeds of approximately 5.7 km/d were calculated from phase shifts in

the velocity records between moorings at similar depths. These values are comparable to the horizontal and vertical energy transport velocities of 23 and 60 m/d observed in the wake of Hurricane Allen [*Brooks*, 1983]. These estimated horizontal and vertical group velocities for the near-inertial response to Hurricane Isaac were calculated using the average vertical and horizontal length scales and the estimated Brunt-Väisälä frequency. The vertical and horizontal scales of Hurricane Isaac were estimated to be 0.96 and 205 km, respectively. These scales are comparable to the vertical scale of ~1 km and the horizontal scale of 370 km determined for Hurricane Allen [*Brooks*, 1983]. Compared to Hurricane Allen, Hurricane Isaac was a much wider hurricane with an R_{max} of 92.6 km to Allen's 20–40 km R_{max}. Hurricane Allen and Hurricane Isaac had similar translation speeds when crossing over mooring arrays, 3.83 m/s for Isaac, and 3.5 m/s for Allen.

While Moorings 1, 3, and 4 showed propagation of energy into the thermocline over time, the near-inertial energy at Mooring 2 remained in the near-surface layer of the water column above 100 m. The inability for the near-inertial energy to penetrate into the thermocline may be explained by the background relative vorticity in the area near Mooring 2. Near-inertial waves were shown to be stalled in the upper water column in areas of cyclonic circulation due to strengthened vertical shears and entrainment cooling [*Jaimes and Shay*, 2010]. Satellite altimetry figures show a transition region between cyclonic and anticyclonic rotation near Mooring 2 during the passage of Hurricane Isaac. Mooring 2 could have been subjected to a strong cyclonic relative vorticity that the course satellite altimetry products were not able to resolve.

After the passage of Hurricane Isaac, the amplitudes of the near-inertial waves increased then experienced an amplitude minimum before increasing again. Between 4 and 5 inertial periods after the storm, both Moorings 1 and 4 experience an amplitude minimum in the depths between 100 and 200 m. This type of amplitude minimum was also observed in the analysis of Hurricane Ivan [*Teague et al*., 2007] and was explained as possibly being related to a separation of the first baroclinic mode from other modes as suggested by the linear theory of *Gill* [1984].

4.3.1. Frequency Shift

The near-inertial frequency was also shifted above the local Coriolis frequency to 1.11*f* in the wake of Hurricane Isaac. A similar blue shift in near-inertial frequency in response to a hurricane was observed by *Shay et al*. [1998] in the study of Hurricane Gilbert in 1988 and by *Jaimes and Shay* [2010] in the study of Hurricanes Katrina and Rita in 2005. *Teague et al*. [2007], *Shay and Elsberry* [1987], and *Schuster* [2013] also found similar shifts in frequency after Hurricane Ivan in 2004 and Hurricane Frederic in 1979. The observed blue shift in frequency in the near-inertial band suggests a strong influence of the background vorticity field on the near-inertial response. It has been shown that the effective frequency of the near-inertial motion can be shifted above the local Coriolis frequency by the relative vorticity of the mean flow as $f_{eff} = f + \zeta/2$ [*Mooers*, 1975; *Kunze*, 1985].

The relative vorticity for the study region was calculated around the time of Hurricane Isaac and compared with satellite altimetry products. The relative vorticity was calculated from the available current meter records at similar depths. The satellite altimetry figures did not fully align with the observed currents and calculated relative vorticity for the study region. This is due in part to the coarse resolution of the altimetry product combined with smoothing applied to the satellite data. The altimetry products show a transitional region between sea surface heights being above and below the mean sea level near the northeastern region of the mooring array. This transitional region could explain some of the discrepancies found between the relative vorticity estimates derived from the current meter records and the expected current directions implied from the satellite altimetry products.

4.4. Subinertial Response

The observed subinertial response to Hurricane Isaac was fundamentally different than the near-inertial response. The subinertial response was strongly barotropic and observed through the entire water column immediately after the passage of the storm. Wavelet analysis showed two distinct subinertial responses, one with a period of 2–5 days and another with a period of 5–12 days. The propagation direction and scales of these waves were unable to be determined from the current meter data available in this study. No clear propagation direction could be determined implying that these subinertial wave were nonvertically propagating. Analysis of sea level height derived from pressure data collected on each ADCP indicated that changes in sea level height associated with each band during the time of Hurricane Isaac's passage aligned

with increased in variability in each band. This is also suggestive of a barotropic response, however, additional analysis is required to quantify this and is beyond the scope of this paper.

Other studies observed similar subinertial responses to hurricanes. A subinertial wave with a period between 2 and 5 days was observed in response to Hurricane Ivan in 2004 [*Teague et al*., 2007]. This study concluded that the subinertial wave could be a topographic Rossby wave based on the propagation direction, bottom intensification, and highly correlated and nearly in phase currents below 150 m. A subinertial wave with a period between 2 and 10 days was observed in the poststorm relaxation stage of tropical Cyclone Gonu in the northern Arabian Sea in 2007 [*Wang et al*., 2012]. Another prominent subinertial wave with a period of 12.7 days was also measured after tropical Cyclone Gonu. This 12.7 day subinertial wave had characteristics of baroclinic topographically trapped waves. A modal decomposition of M1 was performed on the current data set during a time of relatively constant flow parameters (September 2012 to February 2013), which resulted in the identification of a 4–5 day topographic Rossby wave [*Kuehl et al*., 2014]. This result suggests that 4–5 day topographic Rossby waves naturally exist on this region of the northern Gulf of Mexico slope, so it is likely that the passage of Hurricane Isaac excited this type of response upon its passing. However, the transient nature of the response prevents confirmation of this assumption. The subinertial response did show highly correlated and nearly in phase currents throughout the water column, and a slight bottom intensification was observed in the current meter data from some moorings, but the propagation direction was unable to be determined for either subinertial wave. The subinertial responses to Hurricane Ivan were likely not a topographic Rossby wave, but perhaps more simply a strong barotropic response. However, further research is necessary to prove this.

5. Conclusions

On 28 August 2012 Hurricane Isaac approached the GISR mooring array and passed directly over the mooring field with Moorings 1–3 on the right side of the storm path, and Moorings 4–6 on the left side. Relative vorticity was estimated for each side of the hurricane track from available current meter records at similar depths. Before the arrival of Hurricane Isaac, strong negative vorticity was observed on the right side of the hurricane track indicating anticyclonic circulation and positive relative vorticity was observed on the right side, indicating cyclonic circulation. The relative vorticity on each side of the hurricane track increased with the passage of the strong cyclonic hurricane, with the strongest increase on the right side. Maximum observed velocities were also stronger on the right side. The rightward bias was also observed in the wind stress analysis.

Analysis of the near-inertial currents showed a strong increase in variability in the upper water column and a slight increase in phase with depth, indicating downward propagation of energy into the thermocline. Horizontal and vertical phase differences were consistent with near-inertial energy propagating away from the hurricane track at approximately 5.7 km/d and downward at approximately 29 m/d. The near-inertial response was stronger at moorings deployed on the right side of the storm path. A shift in the near-inertial frequency above the local Coriolis frequency was observed after 1–2 inertial periods following the passage of the storm and persisted for almost five inertial periods. This "blue" shift of 1.11*f* was observed in the ADCP current records from each mooring; the background relative vorticity was thought to be the cause of this frequency shift.

In addition to the strong near-inertial response, a fundamentally different subinertial response with periods between 2–5 and 5–12 days was observed throughout the water column. The subinertial responses were vertically coherent and in phase. The horizontal and vertical propagation speeds and directions were ambiguous because clear and consistent phase shifts were not observed between current fluctuations at similar depths. The shallower moorings (2 and 4) experienced the strongest response in both subinertial bands. The 2–5 day subinertial band experienced both surface and bottom intensification at most moorings, but the 5–12 day subinertial band experienced a slight surface intensification and little to no bottom intensification. The moorings deployed in deeper water observed an increase in variability, but not to the same degree as the shallower moorings. The differences may be due to the interaction of inertial wave energy with the topography bathymetry of the continental shelf and slope.

This paper provides a three-dimensional description of the full water-column oceanic response to Hurricane Isaac on the slope of the Northern Gulf of Mexico during summer. The inertial and subinertial waves measured are expected to play an important role in the dynamics along the continental slope, perhaps affecting

a large region in the northern Gulf of Mexico during and after the hurricane passage. The extreme currents and waves associated with Isaac are also valuable to the estimate of the design and operational criteria on the slope given the increasing number of offshore structures from the oil/gas industry in the Gulf of Mexico. The study region is centered on the Deep Water Horizon spill site. The results presented might also be useful to oil spill modeling studies when investigating the hurricane influences on the fate and distribution of oil/gas spill residuals.

Acknowledgments

This research was part of the Gulf Integrated Spill Research (GISR) Consortium and made possible by a grant from the Gulf of Mexico Research Initiative (contract SA12-09/GoMRI-006). We thank Alexis Lugo-Fernandez and BOEM for the loan of many of the current meters and mooring flotation used in this study. The authors thank John Walpert and the Geochemical and Environmental Research Group mooring team for performing the mooring construction, deployment, servicing, and recovery operations. The authors also thank the Captain Nicholas Allen and the crew of the *R/V Pelican* for their service during these operations. We thank Robert Leben for altimeter products produced at the Colorado Center for Astrodynamic Research. We thank L. K. (Nick) Shay (RSMAS, Univ. Miami) for useful conversations and insights into ancillary observations collected during Hurricane Isaac. Data used in this study are publicly available through the Gulf of Mexico Research Initiative Information & Data Cooperative (GRIIDC) at https://data.gulfresearchinitiative.org (UDI: R1.x137.130:0006, R1.x137.130:0010, R1.x137.130:0011, R1.x137.130:0012, R1.x137.130:0011).

References

Bender, L. C., and S. F. DiMarco (2009), *Quality Control Analysis of Acoustic Doppler Current Profiler Data Collected on Offshore Platforms of the Gulf of Mexico*, pp. 90, Texas A&M Univ., College Station.

Bender, M. A., I. Ginis, and Y. Kurihara (1993), Numerical simulations of tropical cyclone-ocean interaction with a high-resolution coupled model, *J. Geophys. Res.*, *98*(D12), 23,245–23,263, doi:10.1029/93JD02370.

Berg, R. J. (2013), Tropical cyclone report Hurricane Isaac, *Rep. AL092012*, U.S. Department of Commerce, 78 pp., National Hurricane Center, Miami, Fla. [Available at http://www.nhc.noaa.gov/data/tcr/AL092012_Isaac.pdf.]

Black, P. G., E. A. D'Asaro, W. M. Drennan, and J. R. French (2007), Air-sea exchange in hurricanes: Synthesis of observations from the coupled boundary layer air-sea transfer experiment, *Bull. Am. Meteorol. Soc.*, *88*(3), 357.

Bloomfield, P. (1976), *Fourier Analysis of Time Series: An Introduction*, 360 pp., John Wiley, N. Y.

Brooks, D. A. (1983), The wake of Hurricane Allen in the western Gulf of Mexico, *J. Phys. Oceanogr.*, *13*(1), 117–129.

Church, J. A., T. M. Joyce, and J. F. Price (1989), Current and density observations across the wake of Hurricane Gay, *J. Phys. Oceanogr.*, *19*(2), 259–265, doi:10.1175/1520-0485(1989)019<0259:Cadoat>2.0.Co;2.

DiMarco, S. F., and R. O. Reid (1998), Characterization of the principal tidal current constituents on the Texas-Louisiana shelf, *J. Geophys. Res.*, *103*(C2), 3093–3109, doi:10.1029/97JC03289.

DiMarco, S. F., M. K. Howard, and R. O. Reid (2000), Seasonal variation of wind-driven diurnal current cycling on the Texas-Louisiana Continental Shelf, *Geophys. Res. Lett.*, *27*(7), 1017–1020.

Emery, W. J., and R. E. Thomson (2001), *Data Analysis Methods in Physical Oceanography*, edited by R. E. Thomson, Elsevier, Amsterdam.

Gill, A. E. (1984), On the behavior of internal waves in the wakes of storms, *J. Phys. Oceanogr.*, *14*(7), 1129–1151.

Grinsted, A., J. C. Moore, and S. Jevrejeva (2004), Application of the cross wavelet transform and wavelet coherence to geophysical time series, *Nonlinear Processes Geophys.*, *11*(5–6), 561–566.

Hamilton, P. (1990), Deep currents in the Gulf of Mexico, *J. Phys. Oceanogr.*, *20*(7), 1087–1104, doi:10.1175/1520-0485(1990)020<1087:Dcitgo>2.0.Co;2.

Huang, S. M., and L. Y. Oey (2015), Right-side cooling and phytoplankton bloom in the wake of a tropical cyclone, *J. Geophys. Res. Oceans*, *120*, 5735–5748, doi:10.1002/2015JC010896.

Jaimes, B., and L. K. Shay (2009), Mixed layer cooling in mesoscale oceanic eddies during Hurricanes Katrina and Rita, *Mon. Weather Rev.*, *137*, 4188–4207, doi:10.1175/2009MWR2849.1.

Jaimes, B., and L. K. Shay (2010), Near-inertial wave wake of Hurricanes Katrina and Rita over mesoscale oceanic eddies, *J. Phys. Oceanogr.*, *40*(6), 1320–1337, doi:10.1175/2010jpo4309.1.

Jaimes, B., and L. K. Shay (2015), Enhanced wind-driven downwelling flow in warm oceanic eddy features during the intensification of tropical Cyclone Isaac (2012): Observations and theory, *J. Phys. Oceanogr.*, *45*, 1667–1689.

Jaimes, B., L. K. Shay, and G. R. Halliwell (2011), The response of quasigeostrophic oceanic vortices to tropical cyclone forcing, *J. Phys. Oceanogr.*, *41*, 1965–1985, doi:10.1175/JPO-D-11-06.1.

Kuehl, J. J., S. F. DiMarco, L. J. Spencer, and N. L. Guinasso (2014), Application of the smooth orthogonal decomposition to oceanographic data sets, *Geophys. Res. Lett.*, *41*, 3966–3971, doi:10.1002/2014GL060237.

Kunze, E. (1985), Near-inertial wave-propagation in geostrophic shear, *J. Phys. Oceanogr.*, *15*(5), 544–565.

Leben, R. R., G. H. Born, and B. R. Engebreth (2002), Operational altimeter data processing for mesoscale monitoring, *Mar. Geod.*, *25*(1–2), 3–18.

Liu, Y. G., X. S. Liang, and R. H. Weisberg (2007), Rectification of the bias in the wavelet power spectrum, *J. Atmos. Oceanic Technol.*, *24*(12), 2093–2102, doi:10.1175/2007jtecho511.1.

Mooers, C. N. K. (1975), Several effects of a baroclinic current on the cross-stream propagation of inertial-internal waves, *Geophys. Fluid Dyn.*, *6*(3), 245–275.

Müller, P., R. C. Lien, and R. Williams (1988), Estimates of potential vorticity at small scales in the ocean, *J. Phys. Oceanogr.*, *18*, 401–416.

Nelson, C. S. (1977), Wind stress and wind stress curl over the California Current, U.S. Department of Commerce, NOAA Technical Report NMFS SSRF-714, 87pp.

Oey, L. Y., M. Inoue, R. Lai, X. H. Lin, S. E. Welsh, and L. J. Rouse (2008), Stalling of near-inertial waves in a cyclone, *Geophys. Res. Lett.*, *35*, L12604, doi:10.1029/2008GL034273.

Powell, M. D., P. J. Vickery, and T. A. Reinhold (2003), Reduced drag coefficient for high wind speeds in tropical cyclones. *Nature*, *422*(6929), 279–283.

Price, J. F. (1983), Internal wave wake of a moving storm. 1. Scales, energy budget and observations, *J. Phys. Oceanogr.*, *13*(6), 949–965, doi:10.1175/1520-0485(1983)013<0949:Iwwoam>2.0.Co;2.

Price, J. F., T. B. Sanford, and G. Z. Forristall (1994), Forced stage response to a moving Hurricane, *J. Phys. Oceanogr.*, *24*(2), 233–260, doi:10.1175/1520-0485(1994)024<0233:Fsrtam>2.0.Co;2.

Qi, H. B., R. A. Deszoeke, C. A. Paulson, and C. C. Eriksen (1995), The structure of near-inertial waves during ocean storms, *J. Phys. Oceanogr.*, *25*(11), 2853–2871, doi:10.1175/1520-0485(1995)025<2853:Tsoniw>2.0.Co;2.

Sanford, T. B., P. G. Black, J. R. Haustein, J. W. Feeney, G. Z. Forristall, and J. F. Price (1987), Ocean response to a Hurricane. 1. Observations, *J. Phys. Oceanogr.*, *17*(11), 2065–2083, doi:10.1175/1520-0485(1987)017<2065:Ortahp>2.0.Co;2.

Schuster, R. M. (2013), The near-inertial response to Hurricane Ivan, MS thesis, p. 457, Dept. Meteorol. and Phys. Oceanogr., Univ. of Miami, Coral Gables, Fla.

Shay, L. K., and S. W. Chang (1997), Free surface effects on the near-inertial ocean current response to a hurricane: A revisit. *J. Phys. Oceanogr.*, *27*, 23–39.

Shay, L. K., and R. L. Elsberry (1987), Near-inertial ocean current response to Hurricane Frederic, *J. Phys. Oceanogr.*, *17*(8), 1249–1269, doi:10.1175/1520-0485(1987)017<1249:Niocrt>2.0.Co;2.

Shay, L. K., R. L. Elsberry, and P. G. Black (1989), Vertical structure of the ocean current response to a Hurricane, *J. Phys. Oceanogr.*, *19*(5), 649–669, doi:10.1175/1520-0485(1989)019<0649:Vsotoc>2.0.Co;2.

Shay, L. K., P. G. Black, A. J. Mariano, J. D. Hawkins, and R. L. Elsberry (1992), Upper ocean response to Hurricane Gilbert, *J. Geophys. Res.*, *97*(C12), 20,227–20,248, doi:10.1029/92JC01586.

Shay, L. K., A. J. Mariano, S. D. Jacob, and E. H. Ryan (1998), Mean and near-inertial ocean current response to Hurricane Gilbert, *J. Phys. Oceanogr.*, *28*(5), 858–889, doi:10.1175/1520-0485(1998)028<0858:Manioc>2.0.Co;2.

Teague, W. J., E. Jarosz, D. W. Wang, and D. A. Mitchell (2007), Observed oceanic response over the upper continental slope and outer shelf during Hurricane Ivan, *J. Phys. Oceanogr.*, *37*(9), 2181–2206, doi:10.1175/Jpo3115.1.

Torrence, C., and G. P. Compo (1998), A practical guide to wavelet analysis, *Bull. Am. Meteorol. Soc.*, *79*(1), 61–78, doi:10.1175/1520-0477(1998)079<0061:Apgtwa>2.0.Co;2.

Walker, N., R. R. Leben, and S. Balasubramanian (2005), Hurricane forced upwelling and chlorophyll a enhancement within cold core cyclones in the Gulf of Mexico, *Geophys. Res. Lett.*, *32*, L18610, doi:10.1029/2005GL023716.

Wang, Z. K., S. F. DiMarco, M. M. Stossel, X. Q. Zhang, M. K. Howard, and K. du Vall (2012), Oscillation responses to tropical Cyclone Gonu in northern Arabian Sea from a moored observing system, *Deep Sea Res., Part I*, *64*, 129–145, doi:10.1016/J.Dsr.2012.02.005.

Wang, Z. K., DiMarco, S. F., and Socolofsky, S. A. (2016). Turbulence measurements in the northern Gulf of Mexico: Application to the deep-water horizon oil spill on droplet dynamics, *Deep Sea Res., Part I*, *109*, 40–50.

Zhang, X., S. F. DiMarco, D. C. Smith IV, M. K. Howard, A. E. Jochens, and R. D. Hetland (2008), Near-resonant ocean response to sea breeze on a stratified continental shelf, *J. Phys. Oceanogr.*, *39*(9), 2137–2155.

Zheng, Q. N., R. J. Lai, N. E. Huang, J. Y. Pan, and L. W. Timothy (2006), Observation of ocean current response to 1998 Hurricane Georges in the Gulf of Mexico, *Acta Oceanol. Sin.*, *25*(1), 1–14.